Applied Thermal Engineering

Performance analysis of an improved temperature control scheme with cold stored in surrounding rock for underground refuge chamber

--Manuscript Draft--

Manuscript Number:	ATE-D-23-03478R1
Article Type:	Original Research Article
Keywords:	Mine refuge chamber; temperature control; Mine compressed air; cold storage; Surrounding rock
Corresponding Author:	Zujing Zhang Guizhou University Guiyang, Guizhou Province CHINA
First Author:	Zujing Zhang, Ph.D.
Order of Authors:	Zujing Zhang, Ph.D.
	Weishuang Guo, Master
	Ruiyong Mao, Ph.D.
	Liang Ge, Ph.D.
	Xing Liang, Ph.D
	Hongwei Wu, Ph.D.
Abstract:	This article proposed an improved temperature control scheme that combines mine compressed air, ice storage and surrounding rock, for mine refuge chambers. The feasibility of cooling mine compressed air via an ice storage unit was experimentally demonstrated, and the performance and temperature control performance of low-temperature mine compressed air on pre-cooling of surrounding rock were studied by numerical simulation. Results showed that: (i) The ice storage unit cools ventilation with a volume flow rate of 300 m3/h could be cooled to 20℃ from 35℃. For mine refuge chambers with an initial surrounding rock temperature of 35℃, the ambient temperature could be kept below 35℃ within 96 h, after pre-cooling the surrounding rock through continuously ventilating for 30 days at normal time. (ii) During pre-cooling, the surrounding rock temperature drops exponentially over time, and the temperature gradient decreases with ventilation rate and ventilation temperature, but has little to do with initial surrounding rock temperature. However the temperature of pre-cooled surrounding rock changes little when the ratio of ventilation time to non-ventilation time is 53:100 for mine refuge chambers with an initial surrounding rock temperature of 35°C. (iii) For mine refuge chambers with an initial surrounding rock temperature of 32℃ or higher, the economy of the mine compressed air-ice storage-surrounding rock scheme will be reflected when the equivalent surrounding rock is 32℃ or lower.
Suggested Reviewers:	Yiming Xiao, Ph.D. Professor, Chongqing University xiaoyimin1974@126.com
	Yijiang Wang, Ph.D. Associate professor, China University of Mining and Technology yjwang@cumt.edu.cn
	Haiguo Yin, Ph.D. Professor, Xi'an University of Architecture and Technology yinhaiguo@xauat.edu.cn
	Xiangkui Gao, Ph.D. Associate professor, China University of Mining and Technology 1024536944@qq.com
Response to Reviewers:	

Cover letter

16th Aug 2023

Dear Sir/Madam,·

We are submitting our manuscript entitled '*Performance analysis of an improved temperature control scheme with cold stored in surrounding rock for underground refuge chamber*' for your kind consideration of its suitability for publication on ***Applied Thermal Engineering***.

Mine refuge chamber (MRC) provides 96 h or more of safe living space for trapped workers awaiting rescue. For MRCs located in sandstone layer with an ISRT above 27°C, the mine compressed air from ground entering the MRC with a rate of 0.3 m^3/min per capita cannot meet the temperature control requirement. In this work, regarding the MRC with high initial rock temperature, an improved temperature control scheme, combining mine compressed air, ice storage and cold stored in surrounding rock was proposed for MRCs. The possibility of mine compressed air being cooled to a lower temperature was determined by experiment. Furthermore, a full-size numerical model of a fifty-person MRC was built and validated. On this basis, the pre-cooling performance of surrounding rock and the temperature control performance of the improved scheme in the MRC were investigated by numerical simulation. In addition, main influencing factors of surrounding rock pre-cooling were analyzed, and the economy of the improved scheme was discussed. The research results can provide theoretical basis for the selection and design of temperature control schemes for high-temperature MRCs.

We hereby confirm that this work has not been submitted to any other journal simultaneously elsewhere. We further confirm that all authors have checked the manuscript and have agreed to the submission.

If you have any other requirement with this submission, please do not hesitate to contact me.

Yours sincerely,
Dr. Zujing Zhang
Guizhou University
Guiyang, Guizhou, China
Tel: +86 185 2391 9513
Email: zjzhang3@gzu.edu.cn

Response to Reviewers' Comments

We do appreciate for the invitation to resubmit our manuscript and the comments for revisions. The manuscript has now been carefully revised according to the reviewers' comments. The comments are very helpful for us to improve the quality of the paper and make it more logical and comprehensive. Please see our point-by-point response to the reviewer's comments as below:

Manuscript number: ATE-D-23-03478
Performance analysis of an improved temperature control scheme with cold stored in surrounding rock for underground refuge chamber

Editor's comments (compulsory)

1. Manuscripts submitted to ATE are expected to be written in good English and proof read carefully to ensure that research is communicated clearly. If necessary, it is suggested that professional editing services may be used; see the following site:

http://webshop.elsevier.com/languageservices/languageediting/?gclid=CNvjjJPwv9MCFQe2wAod01AM7A

Authors' response: Thanks for the comment. We have now carefully checked and improved the English writing thoroughly to avoid any grammatical mistakes and typo errors as well.

2. Check that you have provided 3 to 5 'Highlights' in the form of bullet points, with a maximum of 85 characters, including spaces, per bullet point. Highlights should state clearly the novel outcomes of the study.

Authors' response: Done as requested. We have now revised the highlights to reflect the novelty of the current study.

3. Avoid using abbreviations in the Title, Highlights, Abstract and Conclusions, if possible.

Authors' response: Done as requested.

Reviewer #1: The authors of the entitled manuscript "Performance analysis of an improved temperature control scheme with cold stored in surrounding rock for underground refuge chamber." I found the topic interesting and worth investigating; whilst recognising that the non-renewables mining industries are being phased out in developed countries. I would like the authors to consider and address the following points:

1. Expand the acronym ISR in the abstract and please ensure to define all acronyms in a nomenclature section.

Authors' response: Done.

2. There are many acronyms in the abstract, which makes it difficult to read.

Authors' response: We have now removed the acronyms in the abstract.

3. The current introduction section omitted details on the current computational methods/software used to analyse temperature control.

Authors' response: Thanks for the comment. In the revised manuscript, we have now added detailed information on the current computational methods/software for analyzing the temperature control in the introduction section. Please see page 3, lines 33-40, and page 4, lines 1-13

4. Under section 2.2.5, point (2), why was the water level set to 0.85 m high?

Authors' response: Sorry for the misunderstanding. In the current work, it means to fill the tank with 85% water, not to set the water level to 0.85m. Since the volume of the water frozen into ice will expand, the tank is only 85% full, so that 15% of the expansion space is reserved during the water freezing process.

5. Why do the ventilation and natural convection have different time steps? Also, what was the initial condition?

Authors' response: Thanks for the comment. It is noted that the time step is related to the air velocity and minimum grid size, thus, the air velocity of ventilation and natural convection is different, the time step is different.

The initial conditions for ventilation are: the surrounding rock is pre-cooled at an inlet air velocity of 6 m/s and a temperature of 20℃. The initial conditions of natural convection: the inlet air velocity is 0 m/s, which is an insulated wall, and the air in the chamber flows by gravity and heat pressure.

6. State which software was used for the numerical/computational analysis.

Authors' response: In the current study, Fluent software was used for numerical calculations. Please see page7, line 33-35 and page 8, line 8-15.

7. How long did the simulation take to achieve results for 4.5 hours?

Authors' response: The computer used for numerical calculation is equipped with a 24-core processor and a Tesla GPU with 8 G of memory, and the numerical calculation takes about 4 hours, of which natural convection takes about 2 hours and ventilation takes about 2 hours.

8. On page 14, line 16: The sentence is unclear and requires rewriting.

Authors' response: Done.

9. How were the data, specifically that for natural convection, that were presented in Figure 16 obtained?

Authors' response: The data of natural convection are obtained through numerical simulation.

10. Page 16, line 5: How did the system achieve a recovery ratio of 54%?

Authors' response: Thanks for this comment. First, it should be corrected that the recovery ratio should be 53% instead of 54%. After precooling the surrounding rock for 30 days, the average temperature of the surrounding rock within 1.5m could be reduced by 3.31℃, and after the precooling of the surrounding rock was completed, the average temperature of the surrounding rock within 1.5m increased by 1.74℃ after 30 days of heat exchange in the chamber through natural convection. The ratio of the temperature at which the surrounding rock recovers to the temperature at which the surrounding rock pre-cooling down is called the recovery rate.

11. Page 17, line 4: Please provide a reference that supports using the value of 2.07 x10^6 KJ (total heat dissipation).

Authors' response: A new reference has been added to reflect this comment in the revised manuscript.

12. Page 18, Figure 17, What about the cost of installation?

Authors' response: Compared with the existing ISAC, MCA-ISAC saves the installation cost of explosion-proof fans and explosion-proof batteries, but increases the installation cost of MCA pipeline. Therefore, the actual installation cost is basically the same. In the revised manuscript, we have now supplemented the installation costs in Table 3, Please see page 20, tables 3 and lines 10-12 for details.

13. This paper requires a professional proofreader.

Authors' response:Thanks for the comment. This article has been professionally proofread.

Reviewer #2: The paper has presented an innovative and comprehensive study on temperature control in high-temperature mine refuge chambers (MRCs). The proposed improved temperature control scheme, which combines mine compressed air (MCA), ice storage (IS), and surrounding rock (SR), demonstrates a practical approach to address this crucial problem. The experimental demonstration of cooling MCA using an IS unit provides strong evidence for the feasibility of the proposed scheme. Additionally, the numerical simulations conducted to investigate the SR pre-cooling performance and temperature control performance contribute valuable insights to the field. The findings regarding the temperature reduction in the MCA and the maintenance of ambient temperature within a desirable

range for an extended duration are particularly noteworthy. The paper has effectively conveyed the key results, emphasizing the impact of ventilation rate (VR), ventilation temperature (VT), and initial SR temperature (ISRT) on the temperature control scheme. **Overall, this paper makes a significant contribution to the field, providing valuable insights for the design and operation of MRCs.**

Authors' response: Thank you very much for the reviewer to summarize our work in a very positive way.

Reviewer #3: The paper compares numerical and experimental results on the case interesting for the audience of ATE. However there are some shortcomings the authors need to address first, before the paper could be suggested for publication. The following comments could be the base for a minor revision of the manuscript.

1. Figures should be better designed specifically for this paper, rather than using available figures. Some figures such as experimental figure or the one regarding numerical grid design, are hard to understand and be read.

Authors' response: Thanks for the comment. We have now improved and supplemented the experimental plots in the revised manuscript and make the figure for the numerical grid design to be easily understood. Please see Fig 2 (b), Fig 3 (b), Fig 5 and Fig 6 and Fig16.

2. Please explain what is the physical reason for the offset seen between the numerical and experimental results in Fig. 5.

Authors' response: In the current work, since the ventilation temperature and velocity remain constant when conducting numerical simulation, whereas during the experiment, the Ventilation temperature and ventilation speed fluctuate and are difficult to keep constant. Therefore, there is an offset between the numerical results and experimental data.

3. Quality of Fig. 6 is extremely low, and it is barely understandable.

Authors' response: Corrected. We have now modified Figure 6 to achieve good quality. Please see lines 6-9 on page 12.

4. Please incorporate more detailed findings of the study in the conclusion section.

Authors' response: Done.

5. Reference list is extremely biased in terms of the country where the authors are based. This is a pity and should be certainly addressed.

Authors' response: Thanks for this comment and we agree. In the revised manuscript, many references are cited from different countries.

6. The governing equations of the numerical simulations are not described.

Authors' response: In the revised manuscript, the governing equations have been added. Please see lines8-15 on page 8, lines 5-25 on page 10 and lines 6-8 on page 11.

7. More detailed description of the numerical simulation should be added to the text.

Authors' response: Thanks for the comment. More details regarding the numerical simulation have been added. Please see lines 11-18 on page 8 , lines 5-25 on page 10 and lines 6-8 on page 11.

Performance analysis of an improved temperature control scheme with cold stored in surrounding rock for underground refuge chamber

Zujing Zhang[a,b*], Weishuang Guo[a], Ruiyong Mao[a], Liang Ge[b], Xing Liang[c], Hongwei Wu[d**]

[a] College of Civil Engineering, Guizhou Provincial Key Laboratory of Rock and Soil Mechanics and Engineering Safety, Guizhou University, Guiyang, 550025, China

[b] State Key Laboratory of Gas Disaster Detecting, Preventing and Emergency Controlling, Chongqing Research Institute of China coal Technology and Engineering Group Co. Ltd., Chongqing, 400037, China

[c] School of Computer Science and Mathematics, Kingston University London, KT1 2EE, United Kingdom

[d] School of Physic, Engineering and computer science, University of Hertfordshire, Hatfield, AL10 9AB, United Kingdom

[*]Corresponding author: email: zjzhang3@gzu.edu.cn.

[**]Corresponding author: email: h.wu6@herts.ac.uk.

Abstract: This article proposed an improved temperature control scheme that combines mine compressed air, ice storage and surrounding rock, for mine refuge chambers. The feasibility of cooling mine compressed air via an ice storage unit was experimentally demonstrated, and the performance and temperature control performance of low-temperature mine compressed air on pre-cooling of surrounding rock were studied by numerical simulation. Results showed that: (i) The ice storage unit cools ventilation with a volume flow rate of 300 m^3/h could be cooled to 20℃ from 35℃. For mine refuge chambers with an initial surrounding rock temperature of 35℃, the ambient temperature could be kept below 35℃ within 96 h, after pre-cooling the surrounding rock through continuously ventilating for 30 days at normal time. (ii) During pre-cooling, the surrounding rock temperature drops exponentially over time, and the temperature gradient decreases with ventilation rate and ventilation temperature, but has little to do with initial surrounding rock temperature. However the temperature of pre-cooled surrounding rock changes little when the ratio of ventilation time to non-ventilation time is 53:100 for mine refuge chambers with an initial surrounding rock temperature of 35°C. (iii) For mine refuge chambers with an initial surrounding rock temperature of 32℃ or higher, the economy of the mine compressed air-ice storage-surrounding rock scheme will be reflected when the equivalent surrounding rock is 32℃ or lower.

Key words: Mine refuge chamber; Temperature control; Mine compressed air; Cold storage; Surrounding rock.

Nomenclature

C_p	Specific heat capacity of air, kJ/(kg·k)	***Greek symbols***	
C_1, C_2	Model parameters	ρ	Air density, kg/m^3
$C_{1\varepsilon}$, $C_{3\varepsilon}$	Model parameters	τ	Ventilating time, h
e	Natural base, 2.7182818284	ε	Turbulent energy dissipation, J/(kg·s)
G	Ventilation rate for MRC, m^3/h	β	Coefficient of thermal expansion, 1/K
g_i	Acceleration component of gravity in the i directions, m/s^2	λ	Air thermal conductivity, W/(m·K)
n	Number of IS units	μ	Dynamic viscosity, Pa·s
q	Cold capacity of an ice storage unit, kJ	μ_τ	Turbulent viscosity, Pa·s
Q	Total heat rate in a MRC, W	σ_k	Prandt1 number
Q_m	Cold capacity for a MRC, kJ	σ_ε	Prandt1 number
T_a	Air temperature in MRC, °C	***Acronyms***	
T_{eisr}	Equivalent ISRT, °C	AT	Ambient temperature
T_{isr}	Initial surrounding rock temperature, °C	HR	Heat rate
T_{mca}	Mine compressed air temperature, °C	ISRT	Initial surrounding rock temperature
T_v	Ventilation temperature in MRC, °C	IS	Ice storage
Subscripts		MCA	Mine compressed air
G_b	Generation of turbulence kinetic energy due to buoyancy, J/(s m^3)	MCA-ISAC	IS air conditioner for cooling MCA
G_k	Generation of turbulence kinetic energy due to the mean velocity gradients, J/(s m^3)	MRC	Mine refuge chamber
h	Coefficient in K expression	PCM	Phase change material
i	Coefficient in K expression	SRT	Surrounding rock temperature
j	Coefficient in K expression	SR	Surrounding rock
k	turbulent kinetic energy (J/kg)	VR	Ventilation rate
t	Time s	VT	Ventilation temperature

1 Introduction

Energy storage technology has attracted much attention with rapid development and application of renewable energy [1]. Thermal energy storage systems, including latent heat storage such as phase change material (PCM) device and sensible heat storage such as rock-bed thermal storage system, play an important role in the process of energy storage and application [2,3]. In the field of artificial

environmental control, thermal storage systems can not only promote the application of intermittent or unstable renewable energy such as solar energy, geothermal energy, wind energy, etc., in living and office buildings [4-6], but also make it possible to regulate the artificial environment of some living spaces with air conditioning demand but limited by electrical power such as buildings in remote areas [7,8], data centers [9,10], and underground facilities [11,12].

The mine refuge chamber (MRC) as one of the main safety facilities applied in many countries such as the United States [13], Chile [14], China [15], and Indonesia [16], etc., for underground mines to protect workers against mine disasters. MRC needs to take temperature control measure to keep the ambient temperature (AT) at an acceptable level within 96 h [17-22], and balancing the heat generated from human metabolism and equipment operation as well as high-temperature surrounding rock (SR) [23-25]. During the period of taking shelter, connected to the ground only through a protected air supply pipeline linked to the underground mine compressed air (MCA) system or a vertical borehole from the surface air compressor [26,27]. The rated ventilation rate (VR) for the MCA system is 0.1 m^3/min per capita which needs cover all people in the underground mine, and the rated VR for a MRC is 0.3 m^3/min per capita [28]. However, in order to balance the heat generated by occupants sitting in the MRC, the ventilation temperature (VT) needs to below 15°C when the VR is 0.3 m^3/min per capita, in the case of without considering the heat dissipation influence of the SR [29]. As is normally the case, the SR plays a very important role in determining the temperature control of MRCs [30-32]. When the initial surrounding rock temperature (ISRT) is over 27°C, the MCA with a VR of 0.3 m^3/min per capita cannot maintain the AT less than 35°C within 96 h [25]. Consider increased ventilation costs for MCA systems or the cost of the surface borehole, the economics of the original MCA in cooling the MRC will be significantly reduced for MRCs with high ISRTs [33].

Over the past decade, based on the cold energy storage, several cooling technologies including ice storage (IS) cooling [34-37], PCM cooling [38,39], liquid CO_2 cooling [40] and liquid-air cooling systems [41] have been developed for MRCs. Among them, liquid CO_2 cooling technology can only be used normally in environments where the temperature is below 32°C [42], and the economics of the PCM cooling technology can only be obtained in a MRC with a lower ISRT [38,39]. Although the liquid-air cooling technology is suitable for different temperature environments, its cost is far higher than that of the other technologies [41]. Zhang et al. [43] proposed a novel control temperature scheme that directly connecting the MCA to an IS unit, but it is only applicable to MRCs with an ISRT below 32 °C. Due to SR has good thermal conductivity, high density latent heat storage capacity and is inexpensive, thermal energy storage systems taking SR as heat carrier have attracted more attention in recent years, such as earth-to-air heat exchanger [44,45] and thermal energy storage battery [46] for ground buildings, rock-bed thermal storage systems[47-50]. Bai et al. [51] developed a seasonal heat storage scheme for rock formations, which saves energy for remote mine ventilation through numerical simulation analysis. Zhu et al. [52] used Abaqus software for numerical analysis to proposed a mathematical model of heat regulation and energy storage of SR in a mine tunnel and demonstrated the cooling storage capacity of the SR heat regulation circle. Zhang et al. [53] used

Ansys-Fluent software to proposed a radiation cooling measure by cold the rock wall via heat transfer tubes for high-temperature the underground mine working face.

Nowadays, in terms of temperature control in MRC, attention is being paid to the cold energy stored in SR. Yuan et al. [42] proposed a novel cooling scheme combining cold storage in SR and PCM for MRCs and carried out a semi-analysis to analyze the refrigeration performance of SR. The temperature of the SR and air within the MRC will be pre-cooled at normal times by an available cold source to store a certain amount of cooling and a small amount of PCM. Guo et al. [54,55] developed an ice storage device combining MCA with mixed air supply cooling high temperature MRC, and through experiments and numerical simulations to analyzed the cooling performance of the ice storage device. The results show that during the 96h evacuation period, the ice storage device can control the ambient temperature of MRC with an SRT of 32°C within 35°C. Gao et al. [12,27] combined experimental and numerical studies on the performance of a ground-air heat exchanger for controlling the ambient temperature of MRC. Their result showed that for a MRC buried at a depth of 400 m and with an ISRT of 28.5 °C, the earth-to-air system could maintain the AT below 30 °C within 96 h at a VR of 0.3 m^3/min per capita, but it is not suitable for MRCs buried at depths of more than 400 m. Gao et al. [56] proposed an interchanging continuous and intermittent cold storage strategy for pre-cooling the SR in a MRC, this strategy reduces an annual cold storage energy consumption by 68-78%, compared with the continuous mode.

It is aforementioned from previous studies that for MRCs with high ISRTs, it is difficult to control the indoor AT by the MCA alone, thus cold storage is an effective supplement. This study develops an improved composite temperature control scheme combining the safe and economical MCA-ISAC and SR cold storage with the existing MCA for MRCs with high ISRTs. A set of MCA-ISAC used was fabricated and tested to prove the feasibility of cooling the MCA. Moreover, the thermal performance of cold storage in the SR and the temperature control performance of the improved scheme in MRC were studied in a systematic manner. This study solves the temperature control problem of MRCs with high ISRT, and provides theoretical guidance for the multi-coupled temperature control technology of MRC.

2 Methodology

2.1 Principle of the MCA-IS-SR system

In the current work, an improved temperature control scheme combining MCA with cold energy stored by IS and SR (Abbreviated as MCA-IS-SR) is proposed for MRCs with ISRTs higher than 32°C, as shown in Fig. 1. The MCA pipeline entering the MRC is directly linked to an IS unit, the temperature of the MCA will be cooled through the heat exchange with heat exchanger tubes of the MCA-ISAC. During non-refuge period, the IS unit can operate normally, enough ice will be stored in the MCA-ISAC by running the refrigeration compressor periodically, and the SR temperature (SRT) will be pre-cooled by the cooled MCA to store a certain amount of cold energy. During the refuge period, in case of underground power outage, the temperature control requirement is achieved through the cooled MCA and the pre-cooled SR. The advantage of the improved scheme is that it not only retains the advantages of IS technology and makes full use of the MCA in the absence of underground

electrical power, but also uses the free SR with high potential in energy storage as a cold storage carrier.

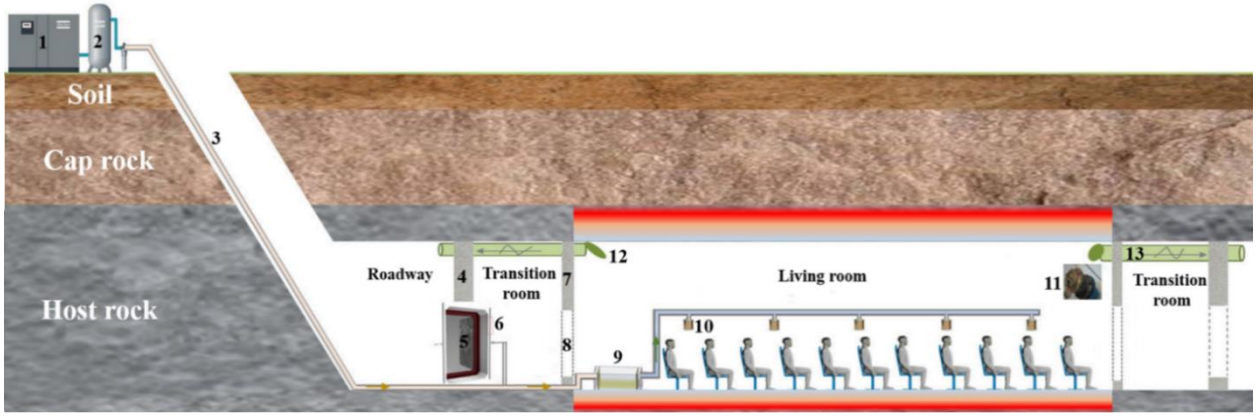

1 - Air compressor, 2 - Air storage tank, 3 - pipeline, 4 - Explosion-protection wall, 5- Protective airtight door, 6 - Air curtain, 7 - Seal wall, 8 - Airtight door, 9 - MCA-ISAC, 10 - Silence air inlet, 11 - One-way exhaust valve, 12 - Air outlet, 13 - Exhaust outlet.

Fig. 1 Principle of the MCA-IS-SR system for high-temperature MRCs.

2.2 Experimental setup

2.2.1 Experimental environment and principle

To test the ability of the MCA-ISAC unit on cooling the MCA, a cuboid MCA-ISAC unit with length, width and height are 1.3 m × 0.7 m × 1.2 m was designed. It is made of 2 mm-thick stainless steel plates and has stress-bearing parts welded inside. The outer wall of the tank is covered with a 30 mm-thick polyurethane insulation material to reduce the heat loss. Circular air inlet and outlet with a diameter of 0.1 m and the air buffer of 0.8 m × 0.5 m × 0.1 m are set at both ends. Between the two air buffers, 18 stainless steel heat exchanger tubes with a length of 1.1 m, an inner diameter of 30 mm and a wall thickness of 2.5 mm are evenly arranged at a horizontal distance of 0.15 m and a height distance of 0.2 m. The copper coiled condenser is submerged inside the tank of the MCA-ISAC unit, then connected to a compression freezer (AOSZGA-040) with a cooling capacity of 5 kW. This can freeze the ice to -30°C and maintain a certain cooling capacity until the temperature of the water in the tank exceeds 20°C. A frequency conversion fan is placed in an artificial environment room with length, width and height are 3.6 m × 3.1 m × 3.0 m, in which the air temperature can be controlled at a relatively stable value in the range of 20 ~ 60 ℃with the assistance of a ventilation heat exchange system. The fan can control the pipeline air speed in the range of 0 ~ 30 m/s, the fan is connected to the air inlet of the IS unit outside the artificial environment room by a steel pipe with a diameter of 0.1 m. The hot air in the artificial environment room is sent to the heat exchange tube of the MCA-ISAC unit through the fan airflow guidance, and after cooling, it flows into the external environment form the air outlet. The experimental principle and experimental environment are shown in Fig. 2 (a) and (b), respectively.

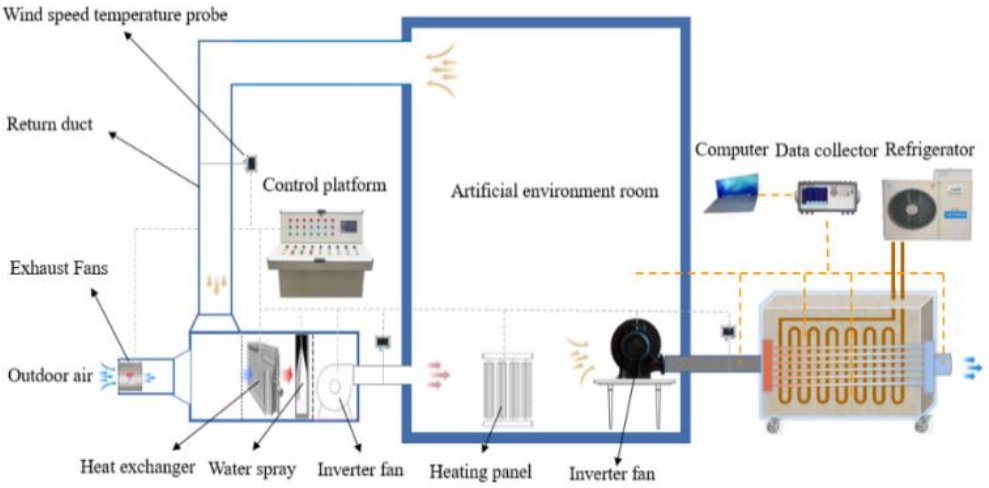

(a) Experimental principle

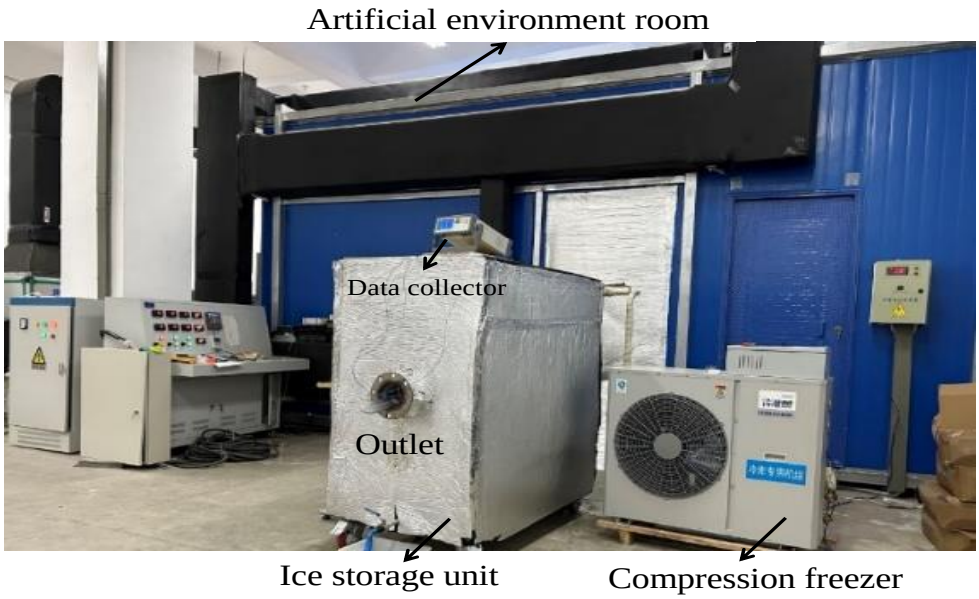

(b) Experimental environment

Fig. 2 Experimental principle and environment for the MCA-ISAC unit.

2.2.3 Data collection

To test the air speed and temperature at the air inlet, a plug-in pipe measuring instrument that can measure the air speed and temperature is fixed on the inlet air supply pipe. In the current work, the air speed is in the range of 0~20 m/s with an accuracy of 0.1 m/s, while the temperature ranges from 0°C to 60°C with an accuracy of 0.1°C. In order to make the inlet air temperature more accurate, a temperature monitoring point was allocated to the inlet air supply pipe. There are 3 temperature monitoring point located at the air outlet to measure the outlet air temperature, and a portable anemometer is used to measure the air speed at the air outlet. In the IS tank, 6 temperature monitoring points are arranged at the level of 0.3 m and 0.9 m above the bottom, and 8 temperature monitoring points are arranged at the 0.6 m level. The K-type thermocouples with a measurement range of 0~200°C and an accuracy of 0.01°C are used to measure the temperature. The measurement data will be automatically recorded per minute and saved every 5 minutes by a data acquisition.

2.2.4 Design of experimental cases

During the refuge period, the heat dissipation rate is about 120 W per capita [24]. The tank has

a volume of about 1 m^3, its cold storage capacity is around 4.14×10^5 kJ including sensible heat of 1.06×10^5 kJ and latent heat of 3.08×10^5 kJ. Assuming that the air supply rate is the rated value of 0.3 m^3/min per capita and the indoor AT is maintained at 35 °C, the cold capacity stored by the MCA-ISAC unit can balance the heat capacity of about 10 people within 96 h without considering heat exchange between SR and air. Practically, the heat exchange between the air and SR can have an important effect on the indoor air temperature control. In a MRC with an ISRT of 30°C, according to the AT prediction method in the ref. [43], the MCA cooled by an MCA-ISAC unit will meet the temperature control requirement of about 17 people. The air supply rates for 10 and 17 people are 3 m^3/min and 4.5 m^3/min, respectively, and their corresponding speeds at the air inlet of the IS unit are 6.37 m/s and 10.82 m/s. Table 1 lists the parameters of the current experimental cases.

Table. 1 Parameters of experimental cases

Case	Inlet air speed (m/s)	Inlet air temperature (°C)	Initial temperature of tank (°C)	Time (h)
1	7	35	-25	96
2	11	30	-28	96

2.2.5 Experimental procedure

The main experimental steps are as follows:

(1) Fix the temperature sensor at the corresponding points in the MCA-ISAC tank, then turn on the temperature data collector to ensure the reliability of data acquisition.

(2) Add water to the tank until it reaches the water level at 0.85 m high.

(3) Run the refrigeration unit until all measuring point temperatures are below -25°C.

(4) Turn on the heating equipment for the artificial environment control room, and maintain the fresh air entering the room at approximately 35°C.

(5) Turn on the frequency fan to make the hot air enter heat exchange tubes of the MCA-ISAC.

(6) Adjust the air speed in the air duct through the fan inverter to 7 m/s.

(7) Stop the test after continuous ventilation for more than 96 h.

(8) Repeat the above steps to complete experimental case 2.

(9) Record and analyse the experimental data.

2.3 Numerical methodologies

2.3.1 Grid model

A grid model of a 50-person MRC will be established, referring to the internal structure of the MRC laboratory in the ref. [43]. The internal size of the MRC is 20 m in length, 4 m in width and 3 m in height, the thickness of the SR is 8 m. Fifty human bodies with a surface area of 2 m^2 are divided into 4 rows in the living room. At above the ground 1.8 m, there are 5 air inlets with a diameter of 0.075 m and a distance between two adjacent inlets of 3.5 m located on each side. As shown in Fig. 3 (a), at above the floor 2.7 m, there is an air outlet with a diameter of 0.225 m located on each end. The mesh of the computational model of the MRC was generated by ANSYS ICEM and the unstructured mesh was adopted. Taking the grid independence study into account, an unstructured grid model with a mesh number of 3.49 million and a minimum orthogonal quality is selected for the

following numerical analysis, see in Fig. 3 (b).

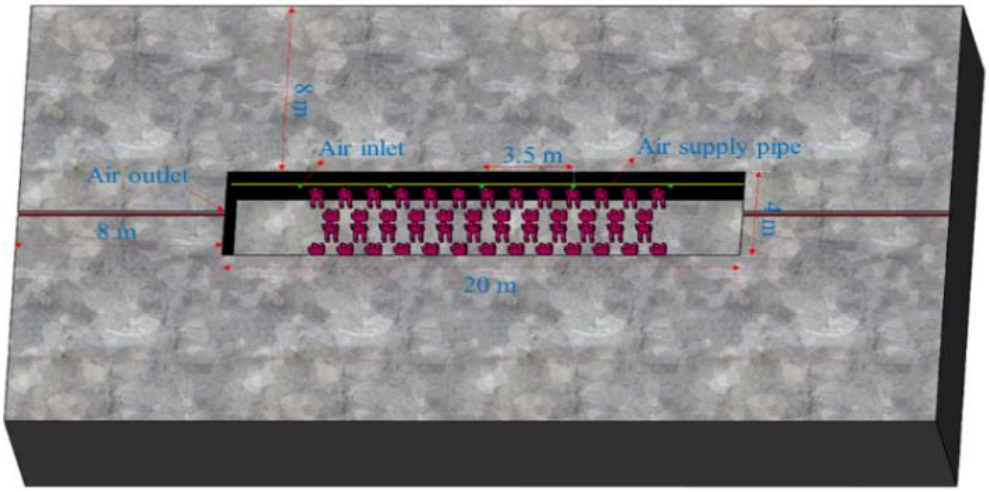

(a) **Geometry model**

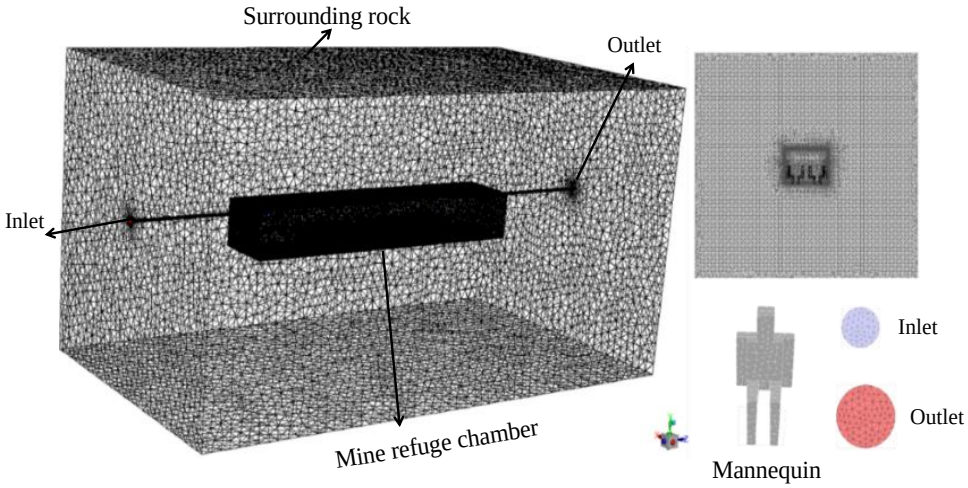

(b) Grid model

Fig. 3 Model of the 50-person MRC.

In the present study, ANSYS Fluent software was used for the numerical simulation. And a mesh independence study was conducted to identify an appropriate mesh density for the aimed calculations. Five meshes were investigated ranging from 2.25 million to 4.32 million cells. The mesh designation and number of cells are shown in Fig 4. compares the average AT value from the numerical calculation at 1 h and 3 h under five different grid models. It can be found that when the grid number is less than 3.49 million, the temperature value at the both moment changes significantly with the increase of the grid number, and when the grid number reaches 3.49 million, the temperature changes little with the increase of the grid number.

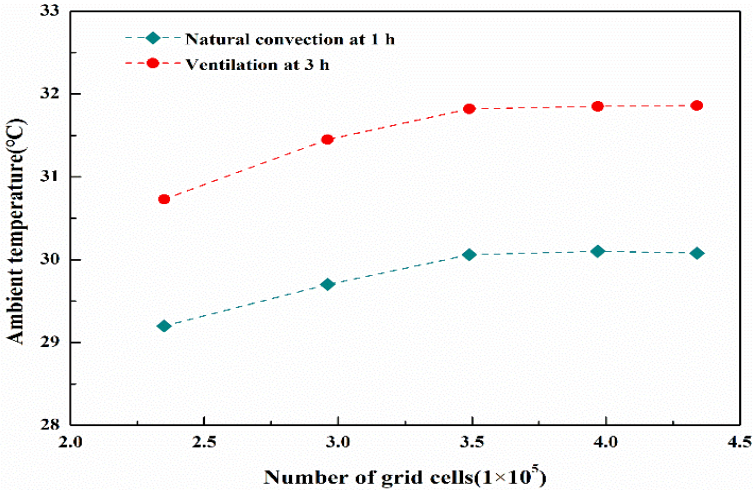

Fig. 4 Comparisons of numerical results under five different grid models.

2.3.2 Initial and boundary conditions

In the current work, a 50-person MRC with an ISRT of 35°C will be selected to analyze the thermal performance of the composite temperature control system. The boundary conditions of the body surfaces, air inlets and air outlets are defined as constant heat flow wall, velocity inlet and outflow, respectively. The surface in contact with the air calculation domain and the surrounding rock calculation domain is set as a coupling wall. Referred to the common SR of MRCs, the thermal conductivity, specific heat capacity and density of the SR are 2 W/(m·K), 920 J/(kg·K) and 2400 kg/m^3, respectively. The heat dissipation rate of occupants in the MRC is 120 W per capita when the refuge period. Separately, the heat flux on body surfaces was 0 W/m^2 during the time of SR pre-cooling and 60 W/m^2 during the refuge period. The VR for the MRC was the rated value of 0.3 m^3/min per capita, And the VT has been cooled to 20°C by the MCA cooling unit. Namely, at a speed of 6 m/s and a temperature of 20°C for all air inlets, the time of pre-cooling SR is 20, 30 and 40 days, respectively, after that, the time of refuge was 4 days.

To analyze the effect of several key impact factors such as ISRT, VR and VT on the performance of pre-cooling SR, the pre-cooling effect of the SR via continuous ventilation for 100 days under different parameters will be compared. The relevant parameters of these numerical cases are listed in Table 2.

Table 2 Parameters setting in numerical cases of SR pre-cooled via continuous ventilation for 100 days

Case 1	ISRT (°C)	VT (°C)	VR (m^3/h)
1	35	20	300
2	35	20	600
3	35	20	900
4	35	20	1200
5	35	20	1500
6	35	16	900
7	35	18	900
8	35	22	900
9	35	24	900

10	32	20	900
11	34	20	900
12	36	20	900
13	38	20	900
14	40	20	900

2.3.3 Turbulent model

Due to the strong performance in airflow, temperature and pressure for closed space [57], the Realizable *k-ε* turbulent model was adopt for the current numerical study. The enhanced wall treatment with pressure gradient effects and thermal effects, as well as the Boussinesq approximation were applied [58]. The governing equations, including continuity equation, momentum equation, and energy equation with Boussinesq, were given as follows [59].

$$\frac{\partial \rho}{\partial t} = -\frac{\partial (\rho u_i)}{\partial x_i} \tag{1}$$

$$\frac{\partial u_i}{\partial t} + \frac{\partial u_i u_j}{\partial x_j} = -\frac{1}{\rho}\frac{\partial P}{\partial x_i} + \frac{1}{\rho}\frac{\partial}{\partial x_j}[\mu(\frac{\partial u_i}{\partial x_j} + \frac{\partial u_j}{\partial x_i} - \rho\overline{u_i' u'}_j) - g_i\beta(T - T_0)] \tag{2}$$

$$\frac{\partial T}{\partial t} + \frac{\partial (u_j T)}{\partial x_j} = \frac{1}{\rho}\frac{\partial}{\partial x_j}(\frac{\lambda}{C_p}\frac{\partial T}{\partial x_j} - \rho\overline{u_i' T'}) \tag{3}$$

where ρ is the air density, kg/m^3; t is the time, s; *xi* and x_j are the Cartesian coordinates in the *i* and *j* directions (*i*, *j* = 1, 2 and 3 corresponding to the *X*, *Y* and *Z* directions respectively); u_i and u_j are the mean fluid velocities in *X*, *Y* and *Z* directions, m/s; u'_i and $u'j$ are the corresponding fluctuant velocity components in the *i* and *j* directions, m/s; *P* is the mean air pressure, Pa; μ is the dynamic viscosity, Pa·s; g_i is the acceleration component of gravity in the i directions, m/s^2; β is the coefficient of thermal expansion, 1/K; *T* is the temperature, K; T_0 is the reference temperature, K; T' is the fluctuating temperature, K; λ is the air thermal conductivity, W/(m·K); C_p is the specific heat capacity, J/(kg·K).

The realizable *k-ε* model consists of the following two transport equations [60].

$$\frac{\partial}{\partial t}(\rho k) + \frac{\partial}{\partial x_j}(\rho k u_j) = \frac{\partial}{\partial x_j}[\frac{\partial k}{\partial x_j}(\mu + \frac{\mu_\tau}{\sigma_k})] + G_b + G_k + \rho\varepsilon \tag{4}$$

$$\frac{\partial}{\partial t}(\rho\varepsilon) + \frac{\partial}{\partial x_j}(\rho\varepsilon u_j) = \frac{\partial}{\partial x_j}[\frac{\partial \varepsilon}{\partial x_j}(\mu + \frac{\mu_\tau}{\sigma_\varepsilon})] + \rho C_1 S\varepsilon - \rho C_2 \frac{\varepsilon^2}{k + \sqrt{\nu\varepsilon}} + C_{1\varepsilon}\frac{\varepsilon}{k}C_{3\varepsilon}G_b \tag{5}$$

where *k* is the turbulent kinetic energy, J/kg; μ_τ is the turbulent viscosity, Pa·s; σ_k and σ_ε are the Prandt1 number; G_b is the generation of turbulence kinetic energy due to buoyancy, J/(s·m^3); G_k is the generation of turbulence kinetic energy due to the mean velocity gradients, J/(s·m^3); ε is the turbulent energy dissipation, J/(kg·s); *S* is the modulus of the mean rate-of-strain tensor; ν is the kinematic viscosity, m^2/s; C_1, C_2, $C_{1\varepsilon}$, $C_{3\varepsilon}$ are model parameters.

In the present study, the pressure-velocity coupling solver and the pressure-implicit with splitting

of operators (PISO) are adopted. The pressure item is discretized by the body force weighted under natural convection and the standard under ventilation, respectively. The other items are discretized by the second-order upwind. Convergence criterion for energy item is 10^{-6}, while it is 10^{-3} for other items. For numerical cases under ventilation, the time step is initially 1 s, then gradually increased to 60 s after convergence. For numerical cases under natural convection, the time step is initially 0.1 s, then gradually increased to 1 s after convergence. It should be noted that the time step is related to the air velocity and minimum grid size, and the time step under ventilation and natural convection conditions is different because the air velocity of the two is different.

2.3.4 Model validation

The numerical model is validated by experimental results in Ref. [43]. The numerical cases of SR and air thermal parameters, thermal rate, ventilation parameters and other parameter settings are consistent with the experimental cases. Fig. 5 plots the comparative curves of the average AT and the deviation varies with time. It can be observed clearly that under three different ventilation states, the average AT obtained by numerical simulation agrees with the experiment data with a temperature difference less than 1°C. The deviation changes from 1.3% to 3.5%, indicating that the error caused by numerical calculation is small, and the numerical model is suitable for the following numerical analyses.

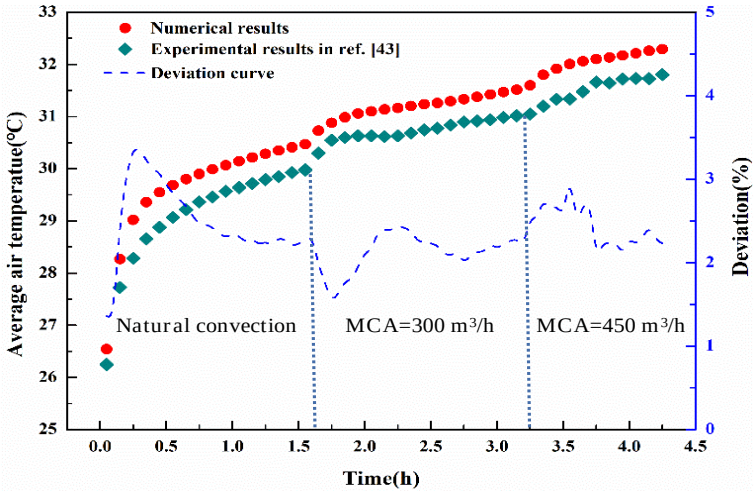

Fig. 5 Comparison of the average AT between experimental and numerical results.

3 Result

3.1 Thermal Performance of cooling MCA

Due to the temperature change of outside air entering the artificial room, the air inlet temperature has a slight oscillation during the process of experimental case 2 and 3, the average air inlet temperature is 36.13°C and 30.39°C, respectively.

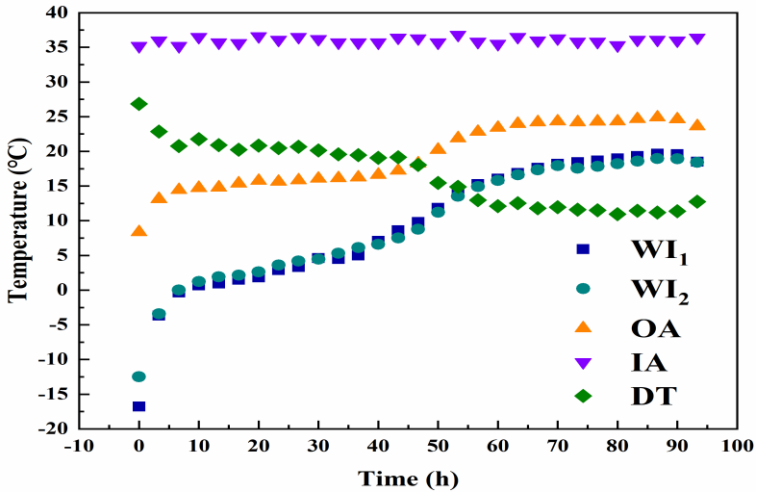

(a) Experimental case 1

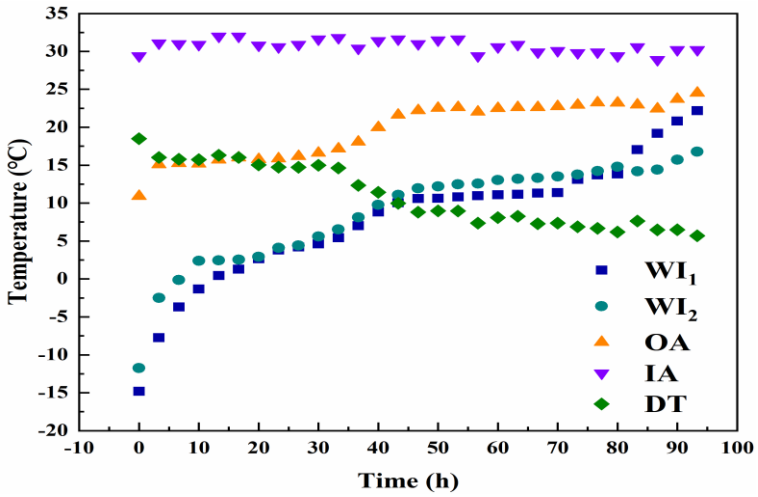

(b) Experimental case 2

Fig. 6 Temperature of the carrier and the MCA varies with time.

Fig. 6 plots the temperature variation of the MCA and the carrier with time within 96 h. In the figure, DT is the temperature difference between the inlet and outlet of the ice storage unit, IA is the inlet temperature, OA is the outlet temperature, and WI_1, WI_2 are the temperature changes in the tank. It can be observed that under a relatively stable air inlet temperature condition, the change in outlet air temperature will go through four stages. The first stage lasts about 6 ~ 8 h, in which the ice does not melt, the outlet air temperature increasing linearly with the time. The second stage lasts about 30 ~ 50 h, during this period there is a slight linear increase in the outlet air temperature over time, the heat of the MCA is absorbed during the melting of ice into water through the latent heat. The third stage lasts about 10 ~ 15 h, in which the outlet air temperature has a rapid linear upward trend, because the ice around the heat exchanger tube has all melted into water, the heat from the MCA is absorbed by water, but it can't be transferred quickly to the ice due to the small contact area between water and ice, resulting in quickly rise of the water temperature. The fourth stage lasts relatively long until all the ice is completely melted, during this period, the outlet air temperature rises slightly, because the ice melting rate has exceeded half, and the heat absorbed by the water can be quickly transferred to the ice through latent heat absorption due to sufficient thermal contact area.

Separately, from Fig. 6 (a) it can be observed that when the inlet air speed is 7 m/s, the temperature of the MRC can be cooled by the IS unit to below 20°C from about 36°C during the first 50 h, accompanying with a temperature difference of over 18°C. In the next 46 h, the outlet air temperature is basically maintained around 25°C. From Fig. 6 (b), it can be observed that when the inlet air speed is 11 m/s, the temperature of MRC can be cooled to below 20 °C from about 30°C during the first 48 h, and its value is less than 23°C in the next 48 h. The experimental results indicate that it is feasible to use the IS unit to cool the MCA, so as to storage cold source by the SR of the MRC during normal time or control temperature during the refuge period.

3.2 Thermal performance of the MCA-IS-SR system

3.2.1 Distribution of AT and SRT during pre-cooling

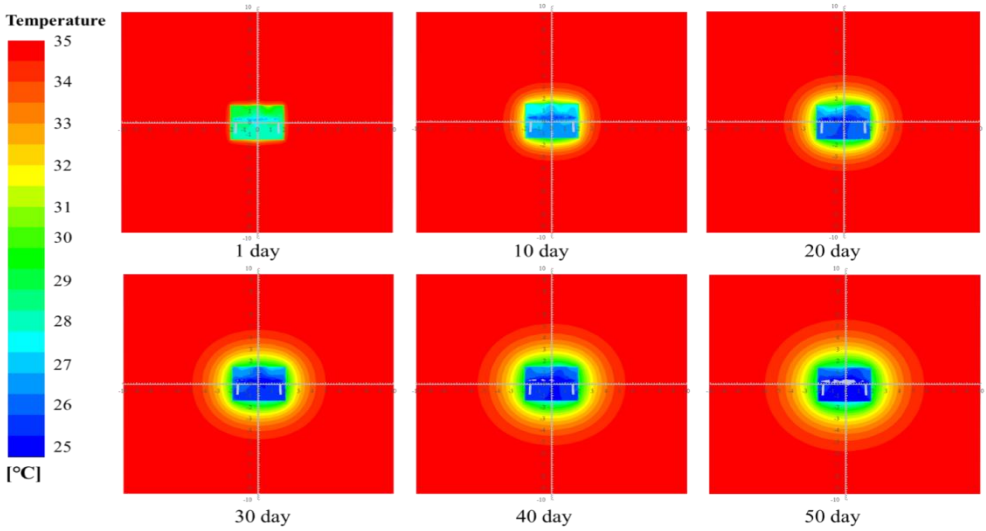

Fig. 7 Variation of the AT and the SRT at different times during pre-cooling

To observe the distribution characters of the AT and the SRT under the action of the cooled MCA with a VR of 900 m^3/h and a VT of 20°C, temperature clouds on the centre section surface of the MRC at different times, i.e., 1, 10, 20 ,30, 40 and 50 days, are compared. Fig. 7 displays the variation of the AT and the SRT under cooled MAC at different times. It can be observed that in the early stages, the AT is higher than the VT, because the air obtains heat in the dynamic heat transfer process between air and SR. With the increase of ventilation time, the AT gradually decreases. As far as the SR is concerned, when the ventilation lasts for a day, the SRT changes small, only a slight increase in temperature near the wall surface. While the ventilation lasts for 10 days, the temperature of the SR within 1 m decreases obviously. When the ventilation lasts for 20 days, the temperature of the SR beyond 1 m from the inner wall decreases in a circle from the inside to the outside, but the intensity gradually decreases, and the temperature variation of the SR beyond 2 m is hardly observed. As the ventilation time increases from 20 days to 50 days, although the SRT continues to decrease, the temperature variation of the SR beyond 3 m is not easy to be observed.

3.2.2 Variation of AT and SRT during pre-cooling

To know the variation of the SRT over time under the action of the cooled MCA with a VR of 900 m^3/h and a VT of 20°C. The SRT at 12 monitoring points varies with time within 50 days are compared. These points are located at 1.5 m above the floor on the centre section of the MRC, apart

from the inner wall surface 0, 0.5, 1, 1.5, 2, 2.5, 3, 4, 5, 6, 7 and 8 m, respectively.

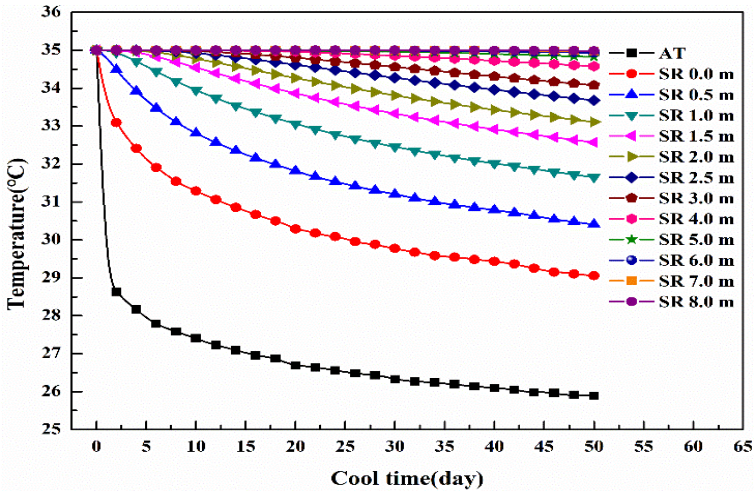

Fig. 8 Variation of the AT and the SRT with pre-cooling time within 50 days.

Fig. 8 plots the average AT and the SRT at different points change with time. It can be found that in the first 2 days, the average AT drops rapidly from 35°C to 28.8°C, then slowly decreases over time and keeps a relative stable temperature difference of 3 ~ 4°C with the SR surface, indicating that the heat transfer process between air and SR has entered a dynamic equilibrium state. The SRT decreases over time, occurring from the inner to outside. When the distance is in the range of 0 ~ 1.5 m, the SRT decreases curve with time, also its gradient decreases over time, because the heat obtained through the heat transfer between air and wall is absorbed by more volume of SR. When the distance exceeds 2 m, the SRT drops approximately linearly with time. With the increase of the distance, the intensity of the SRT drop is weakening. After the ventilation lasts for 5, 10, 20 and 40 days, respectively, the SRT at 1.5, 2.5, 4 and 5 m begins decrease sequentially. However, after 50 days of ventilation, it is still difficult to observe the temperature of SR at the 6 m position drop.

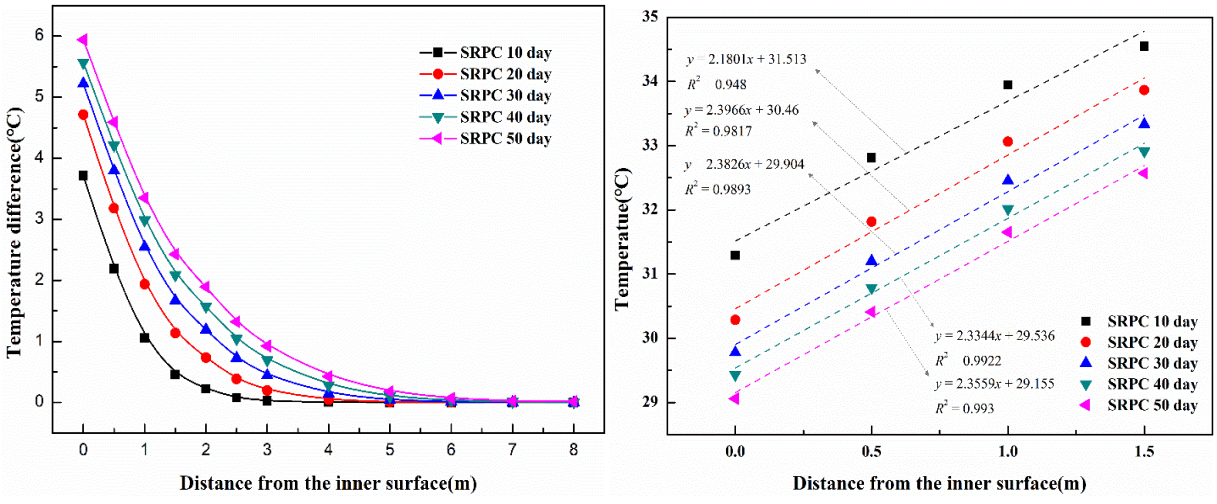

(a) Temperature difference of SR from 0 ~ 8 m at different times (b) SRT from 0 to 1.5 m at different times

Fig. 9 Variation of the SRT with the distance from the inner surface at different times.

Fig. 9 (a) plots the temperature difference of SR from 0 ~ 8 m at different times. It can be observed that at a same moment, the temperature difference of SR decreases exponentially with distance. Among them, from 0 to 1.5 m, the temperature difference decreases the fastest with distance,

which is approximately linear, while the distance is over 3 m, the temperature difference becomes little, indicating that during the pre-cooling time, the cold capacity is mainly stored in the SR within 3 m. At the same point, the longer the ventilation time, the greater the temperature difference of SR. Fig. 9 (b) plots the temperature of SR from 0 to 1.5 m points at five different times. It can be found that during the SR pre-cooling time, the SRT has an obvious linear relationship with the distance within 1.5 m. With the increase of time, the linear relationship becomes much more significant.

3.2.3 Performance of the MCA-IS-SR system during taking shelter

To know the temperature control characteristics of the MCA-IS-SR scheme, the MRC with an ISRT of 35℃ has been pre-cooled by the cooled MCA with a VT of 20℃ and a VR of 900 m^3/h for 30 days. After that, a HR of 6 kW is released from the 50 human body surfaces and the ventilation lasts for 4 days without changing the parameters of ventilation.

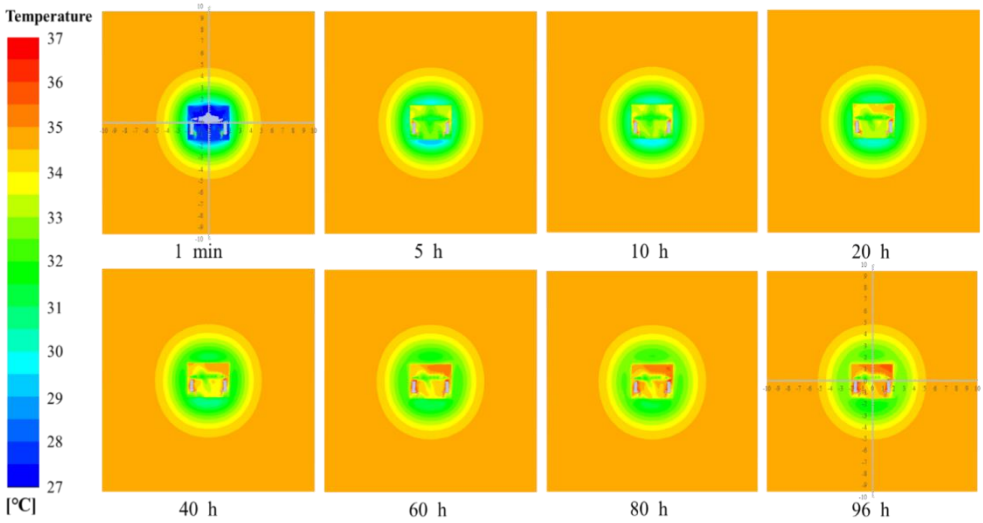

Fig. 10 Distribution of AT and SRT under cooled MAC at different times.

Fig. 10 displays the variation of the AT and the SRT under the cooled MAC at different times during taking shelter. It can be found that at the initial moment, the temperature distribution of the SR is non-uniform and the AT is lower than 28°C. Specifically, the SRT gradually decreases from the inside to the outside in the range of 0 ~ 3 m, and the temperature of the SR beyond 3 m remains constant. For the SR within 1 m apart from the inner wall surface, the bottom has the lowest temperature, followed by the top, while the both-sides has a relatively high temperature. The AT is gradually rising with the increase of time, yet not beyond 35°C overall at the first 40 h. At 60 h, the AT in the upper space reaches 36°C, while in the lower part its value is still below 35°C. At 96 h, the AT in the lower space of human activity is close to 35°C.

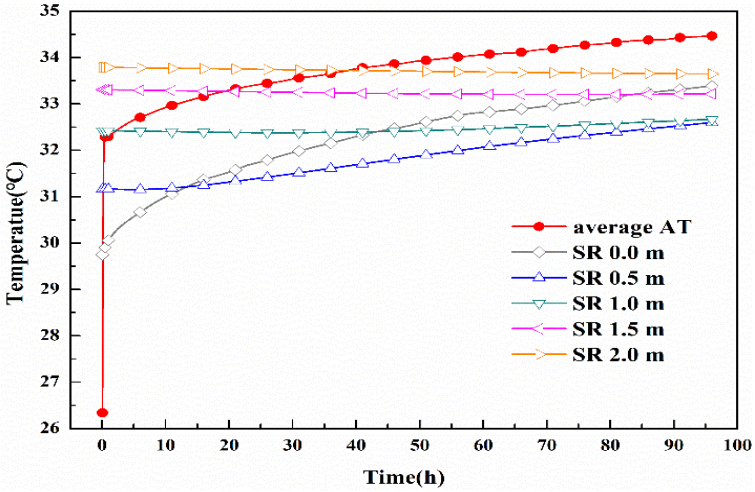

Fig. 11 Temperature varies with time during 96 h of taking shelter.

Fig. 11 plots the average AT and the SRT at different distance varying with time within 96 h. It can be found that although the AT increases gradually with time, it does not exceed 35℃ at 96 h, indicating that the temperature control requirement of the MRC with an ISRT of 35℃ can be met through the MCA-IS-SR scheme. The temperature change trend of the SR on the inner surface is similar to that of the AT. As the distance increases, the temperature change of the SR gradually weakens. The SRT at 1 m increases by about 0.3°C within 96 h. The SRT at 1.5 m still keeps a slight downward trend in the first 80 h, decreasing by about 0.2°C, after that, about 0.1°C is increased in the next 16 h. The SRT at 2 m maintains a slight downward trend within 96 h, dropping by about 0.3°C. It can be concluded that during the 96 h of taking shelter, only the cold energy stored by SR in the range of 1.5 m plays a positive role in the temperature control of the MRC.

3.2.4 Prediction of AT in the MRC during taking shelter

To predict the AT of MRCs with pre-cooled SR during the time of taking shelter, keeping the same ventilation and HR, i.e., the VT is 900 m^3/h, the VT is 20°C and the HR is 6 kW, the AT curves of the MRC with pre-cooled SR and the MRC with equivalent ISRT will be compared. For the MRC with an ISRT of 35°C, after being pre-cooled by the cooled MCA for 20, 30 and 40 days, the equivalent ISRTs are 32.25, 31.7 and 31.27°C, respectively.

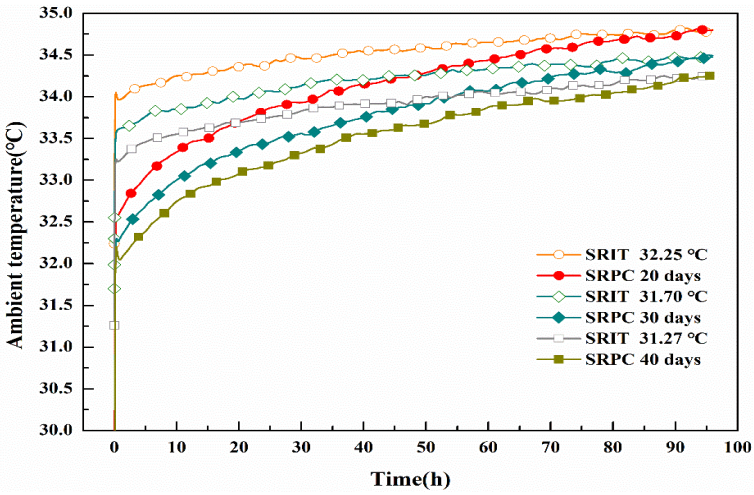

Fig. 12 Comparison of AT varies with time under the three different conditions.

Fig. 12 compares the variation curves of the AT within 96 h for the MRC with the pre-cooled SR and the MRC with the equivalent ISRT under the same ventilation conditions. It can be found that for the three different cases, the AT of the MRC with pre-cooled SR is essentially equal to that of the MRC with the equivalent ISRT at the moment of 96 h. Previously, the MRC with pre-cooled SR has lower AT than the MRC with equivalent ISRT, because the former has a lower temperature near the inner wall surface, which allows more heat from the breathing environment to be absorbed. Overall, for the MRC with pre-cooled SR, the average temperature of the SR within 1.5 m can be regarded as an equivalent ISRT, then the AT of the MRC at the moment of 96 h can be predicted.

3.3 Sensitive analyse during pre-cooling

Since the average temperature of the pre-cooled SR within 1.5 m plays an important role in the temperature control performance of the MRC when taking shelter, the average temperature of SR within 1.5 m varies over time are compared during the SR pre-cooling time.

3.3.1 Effect of the VR

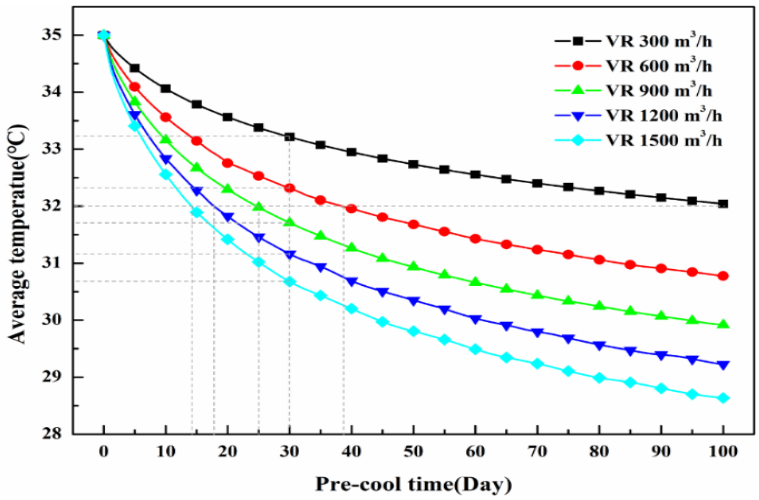

Fig. 13 Average temperature of SR within 1.5 m under different VR.

Fig. 13 plots the average temperature of SR within 1.5 m varies with time under different VR. It can be found that the average temperature drops exponentially over time. With the increase of VR, the gradient of the SRT increases, but the intensity of the gradient increase becomes weaker at the same moment, for example, at 30 days of continuous ventilation by the MCA, the average temperature of the SR decreased by 1.79, 2.69, 3.30, 3.83 and 4.31°C at a VR of 300, 600, 900, 1200 and 1500 m^3/h, respectively. In addition, taking the average SR temperature of 32°C as the cold energy storage target, when the VR is 600, 900, 1200 and 1500 m^3/h, the continuous ventilation time is 38.5, 25, 18 and 14 days, respectively.

3.3.2 Effect of the VT

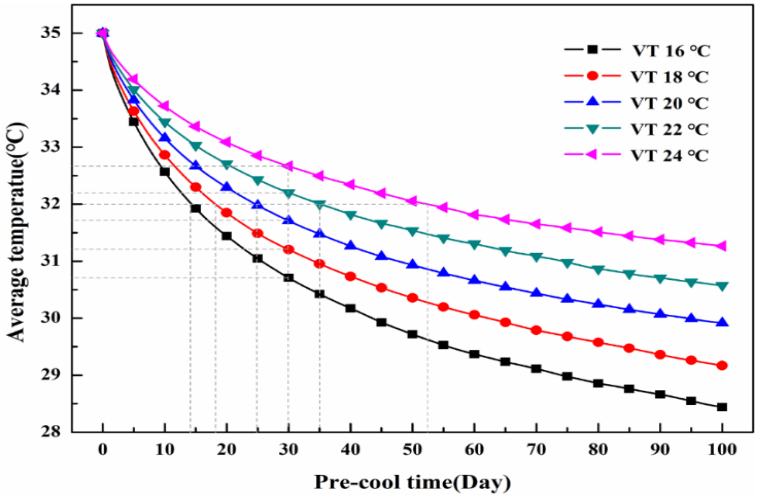

Fig. 14 Average temperature of SR within 1.5 m under different VT.

Fig. 14 plots the average temperature of SR within 1.5 m varies with the cooling time under different VT. It can also be seen that the average temperature of the surrounding rock thickness within 1.5 meters is exponentially related to time and decreases with increasing time. With the increase of VT, the gradient of the SRT decreases, but the intensity of the gradient increase keeps the same at the same moment, for example, at 30 days, the average drop temperature of the SR increases by 0.49 °C for every 2°C increase in VT. Taking the average SR temperature of 32°C as the goal of cold storage, when the VT is 16, 18, 20, 22 and 24°C, the continuous ventilation time is 14, 18, 25, 35 and 52.5 days, respectively.

3.3.3 Effect of the ISRT

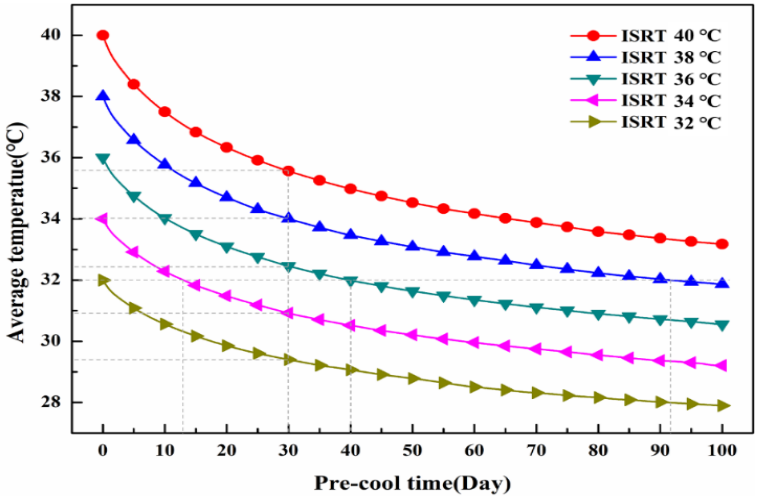

Fig. 15 Average temperature of SR within 1.5 m under different ISRT.

Fig. 15 plots the average temperature of SR within 1.5 m varies with the pre-cooling time under different ISRT. Similarly, it can be found that the average temperature of the SR within 1.5 m drops exponentially with time. However, the ISRT has little effect on the gradient of the SRT drop. At 30 days, the average drop temperature of the SR increases by 1.6°C for every 2°C increase in ISRT. Taking the average SR temperature of 32°C as the goal of cold storage, when the ISRT is 34, 36 and 38°C, the continuous ventilation time is 13, 40 and 92 days, respectively.

3.4 Thermal recovery of the pre-cooled SR

To analyze the thermal recovery performance of the pre-cooled SR, the SR with an ISRT of 35°C has been pre-cooled by continuous ventilation with a VT of 20°C and a VR of 900 m^3/h for 30 days, then exposed to a natural convection environment for 30 days.

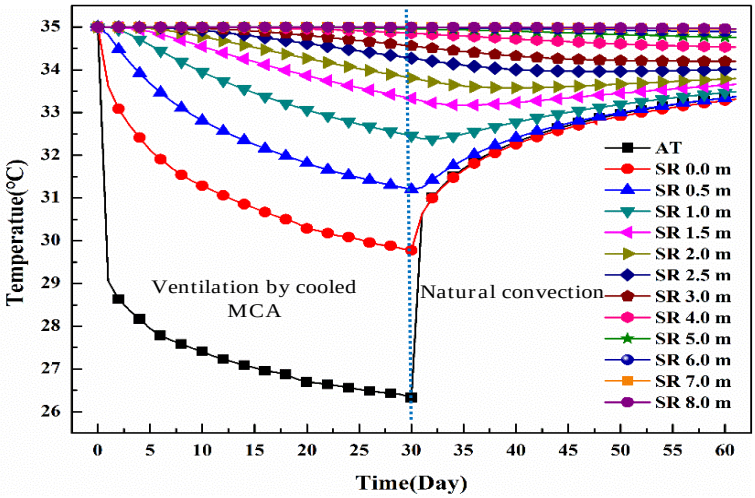

Fig. 16 Temperature variation of the pre-cooled SR with time under natural convection.

Fig. 16 plots the temperature variation curves of SR pre-cooled 30 days varying with time under natural convection. It can be found that under natural convection, the temperature on the surface of the SR has an obvious recovery, and the AT has a similar trend with the temperature on the surface, following with temperature difference less than 0.2°C. As the depth increases, the less the rock temperature recovers. After 30 days of ventilation by cooled MCA, the temperature of rocks at 0, 0.5, 1 and 1.5 m decreased by 5.22, 3.78, 2.55 and 1.67°C, respectively, and the average temperature of SR within 1.5 m decreased by 3.31°C. In contrast, after 30 days of natural convection, the temperature of pre-cooled SR at 0, 0.5 m, 1 and 1.5 m recovered by 3.50, 2.14, 1.01 and 0.31°C, respectively, and the average temperature of SR within 1.5 m recovered by 1.74°C. The ratio of the temperature at which the surrounding rock recovers to the temperature at which the surrounding rock pre-cooling down is called the recovery rate, with a recovery ratio of about 53%, indicating that during the cold preservation period of the pre-cooled SR, when the ratio of ventilation time to non-ventilation time is 53:100, the average temperature of the pre-cooled SR within a depth of 1.5 m can be basically unchanged.

4 Discussion

4.1 Economics of the MCA-IS-SR system

4.1.1 Comparison of a device cost

As available alternative cooling schemes for MRCs, two existing ISACs has been reported, including a forced-circulation ISAC with an ice storage capacity of 5.34 m^3 [34] and a multifunctional ISAC with an ice storage volume of 1.8 m^3 [37]. However, both devices require explosion-proof fans to drive the indoor hot air to flow through the heat exchange channel of the device, then the cooled air return to the indoor environment to achieve the cooling function. In addition, both devices need to be equipped with explosion-proof batteries with sufficient storage capacity to meet the power

consumption needs of explosion-proof fans in 96 h. Compared with the existing two devices, when using the MCA-IS-SR scheme, the cost of MCA-ISAC will be greatly reduced, because it does not need to be equipped with explosion-proof fans and explosion-proof batteries. Meanwhile, the operating and maintenance costs of the equipment will be significantly reduced during the five-year service period, as there is no need to charge the battery and maintain the fan and battery. According to a survey result of market and user, Table 3 compares the critical component cost, operating cost and installation cost between the existing ISAC and the MCA-ISAC, in the case of an ice storage capacity of 1 m^3. It can be known that compared with the price of ¥ 80,000 for the existing ISAC, the price of the MCA-ISAC has decreased by 50%. At the same time, its annual operating costs will be cut in half, about ¥ 3000. Compared with the existing ISAC, MCA-ISAC saves the installation cost of explosion-proof fan and explosion-proof battery, but increases the installation cost of MCA duct, so the actual installation cost is basically the same.

Table 3 Comparison of equipment cost and operating cost between the existing ISAC and the MCA-ISAC

Item	Existing ISAC	MCA-ISAC
Critical component costs	Ice storage tank, ¥ 3000	Ice storage tank, ¥ 3000
	Heat exchange component, ¥ 2000	Heat exchange component, ¥ 7000
	Refrigeration compressor, ¥ 30,000	Refrigeration compressor, 30,000
	Explosion-proof fan, ¥ 10,000	/
	Explosion-proof battery, ¥ 35,000	/
Operating costs	Ice storage process, ¥ 2000 per year	Ice storage process, ¥ 2000 per year
	Battery charging process, ¥ 2000 per year	MCA ventilating process, ¥ 500 per year
	Maintenance, ¥ 2000 per year	Maintenance, ¥ 500 per year
Installation costs	Ice storage unit install, ¥ 2000	Ice storage unit install, ¥ 2000
	Explosion-proof fan install, ¥ 500	MCA duct install, ¥ 1000
	Explosion-proof battery install, ¥ 500	

4.1.2 Comparison of the system cost in MRC

Taking the above 50-person MRC with an ISRT of 35℃ as the object, economics of three temperature control schemes including the existing IS, the MCA-IS and the MCA-IS-SR, will be compared. The total heat dissipation from the human bodies is about 2.07×10^6 kJ within 96 h [24]. Assuming that the AT keeps a constant of 35℃ during the taking shelter time, meaning that there is no heat exchange between the air and the SR.

When the MCA-IS scheme is adopted, the average AT in the MRC after 1 h of ventilation can be calculated as follow [43].

$$T_a(\tau) = [(1.35T_v - 1.3T_{isr} + 4.63Q) \times 10^{-2} + 0.7e^{-0.002G} - 0.16]\sqrt{\tau} + 0.27T_v + 0.7T_{isr} - 0.003G + 0.8Q + 4 \quad (6)$$

Where, T_a is the AT in the MRC, ℃; τ is the ventilating time, h; T_v is the VT, ℃; T_{isr} is the ISRT, ℃; Q is the HR generated by occupants, kJ; G is the VR, m^3/h.

Assuming that the AT of the MRC at 96 h is 35℃, thus, when the VR is 900 m^3/h and the HR is 6 kW, according to eq. (6), the relation between the VT and the ISRT can be written as

$$T_v = 66.78 - 1.45T_{isr} \quad (7)$$

Since the MCA entering the MRC needs to be transported through a long-distance pipeline, the

temperature of the MCA is close to the ISRT. According to Newton cooling law, the required cold capacity for the MRC temperature controlling within 96 h can be calculated as

$$Q_m = \rho C_p G(T_{mca} - T_v)\tau = 96\rho C_p G(T_{isr} - T_v) = (2.73T_{isr} - 74.43) \times 10^5 \quad (8)$$

Where, Q_m is the cold capacity for a MRC, kJ; T_{mca} is the temperature of MCA entering the MRC, ℃.

Furtherly, the number of IS units for the MRC is calculated as

$$n = Q_m/q \quad (9)$$

Where, n is the number of IS units for MRC; q is the cold capacity of an IS unit, kJ.

It can be calculated from eq. (8) and (9) that, for the 50-person MRC with an ISRT of 35℃, also about 5 IS devices are required when the MCA-IS scheme is adopted. The cost of the MCA-IS system is ¥ 265,000, consisting of ¥ 250,000 in equipment cost and ¥ 15,000 in operating cost during 5-year service period, which is about 38% less in the cost than the existing IS system.

When the MCA-IS-SR scheme is adopted, assuming that the SRT has been pre-cooled to the equivalent ISRT, in the case of a VR of 900 m^3/h, the relationship between the VT and the equivalent ISRT is expressed as follow

$$T_v = 66.78 - 1.45\,T_{eisr} \quad (10)$$

Where, T_{eisr} is the equivalent ISRT, ℃.

Assuming that the T_{mca} is equal to the ISRT, for the MRC with an ISRT of 35℃, according to Newton cooling law, the required cold capacity for the MRC temperature controlling within 96 h can be calculated as follow

$$Q_m = \rho C_p G(T_{mca} - T_v)\tau = (1.616\,T_{eisr} - 35.421) \times 10^5 \quad (11)$$

According to Eqs. (9) and (11), when the equivalent SRT was pre-cooled to 32.2℃ and 29.6℃ after 22 days and 110 days, respectively, the number of devices was reduced to 4 and 3 for the MRC with an ISRT of 35℃ to meet the temperature control requirement within 96 h.

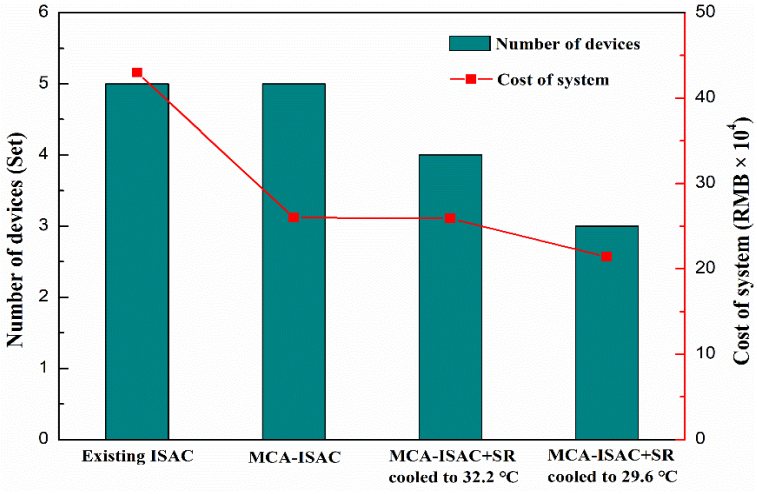

Fig. 17 Economic comparison of different cooling schemes

Fig. 17 compares the cost of the temperature control system over a five-year period of service under different temperature control schemes. It can be found that when the SR is not used as a cold storage medium, although the number of devices required for the existing ISAC scheme and the MCA-ISAC scheme is the same, the cost of the latter is reduced by ¥ 170,000, a reduction of about 40%. When the MCA-ISAC-SR is adopted, the number of devices will be reduced to 4 after the SR

is pre-cooled to an equivalent temperature of 32.2℃ from the ISRT of 35℃. Whereas, compared to the MCA-ISAC scheme, its cost only decreases by about 0.4%, because the cost of cold storage via the SR and maintenance over a five-year service period is close to the cost of one device. Furthermore, by pre-cooling the SR to an equivalent temperature of 29.6℃, the number of devices will decrease to 3, resulting in a cost reduction of approximately ¥ 46,000 with a decrease of about 17.7%, compared to the MCA-ISAC scheme. It can be deduced that for MRCs with an ISRT of 32℃ or more, the economy of the MCA-IS-SR scheme will reflect after the SR is cooled to equivalent 32℃ or below.

4.2 Cooling schemes for MRCs with different ISRT

Thanks to the cold radiation of the low-temperature SR, cooling measures are not necessary for MRCs with an ISRT of 20°C or less [61]. When the VR is 0.1 m^3/min per capita for a MRC, the CO_2 concentration, O_2 supply and the RH can be kept at the safe level [24,28,29], even more, the AT cannot over 35°C at 96 h if the ISRT is not more than 25°C [25]. When the VR is 0.3 m^3/min per capita, the MCA can keep the AT of the MRC below 35°C under the condition that the ISRT is below 27°C [27]. While the VR reaches 0.5 m^3/min per capita, the MCA can meet the temperature control requirement of the MRC with an ISRT of 30°C, according to eq. (11). Practically, for most MRCs, the VR will not more than 0.3 m^3/min per capita, so the temperature control scheme of MCA-IS was recommend for MRCs with ISRT above 27°C [43]. However, considering the cost, the improved temperature control scheme of MCA-IS-SR is more worthy of promotion for MRCs with an ISRT of above 32°C. The temperature control scheme for MRCs with different ISRT can refer to Table 4.

Table 4 Economical temperature control scheme for a MRC with different ISRTs.

ISRT of the MRC	Recommended scheme	Air supply volume per capita (m^3/min)	Number of people served by each ISD
20°C or less	Not required	0.1	/
20 ~ 25°C	MCA	0.1	/
25 ~ 27°C	MCA	0.1 ~ 0.3	/
27 ~ 30°C	MCA	0.3 ~ 0.5	/
	& MCA-IS	0.3	20 ~ 25
30 ~ 32°C	MCA-IS	0.3	15 ~ 20
32°C or more	MCA-IS-SR	0.3	10 ~ 15

5 Conclusion

An improved composite temperature control scheme combining MCA, IS and SR was proposed for MRCs with high ISRT. The feasibility of using IS unit to cool the MCA was tested. On this basis, thermal performance of the improved scheme applied to MRC with high ISRT was studied by numerical simulation. In addition, the economy of the improved scheme was discussed. The following specific conclusions can be drawn:

(1) It is feasible to use the ice storage unit to cool the mine compressed air, the mine compressed air temperature will reduce by 15 ~ 18°C at the first 30 h and by 6 ~ 8°C within 40 ~ 96 h when the air volume is 300 m^3/h.

(2) With the increase of distance, the intensity of surrounding rock temperature drop is

weakening, the surrounding rock temperature within 1.5 m decreases approximately linearly with the distance, which can be regarded as an equivalent initial surrounding rock temperature to predict the ambient temperature of the mine refuge chamber at 96 h.

(3) For a mine refuge chamber with an initial surrounding rock temperature of 35°C, when the ventilation temperature is 0.3 m^3/min per capita and the ventilation temperature is 20°C, the average ambient temperature can maintain below 34.5°C within 96 h, after the surrounding rock has been pre-cooled by continuous ventilation for 30 days.

(4) During pre-cooling, the surrounding rock temperature drops exponentially over time, the temperature gradient decreases with the ventilation rate and the ventilation temperature, but has little to do with the initial surrounding rock temperature. The temperature of the pre-cooled surrounding rock changes little when the ratio of ventilation time to non-ventilation time is 53:100.

(5) After 30 days of ventilation by cooled MCA, the average temperature of SR within 1.5 m decreased by 3.31℃. After 30 days of natural convection, the average temperature of SR within 1.5 m recovered by 1.74℃, with a recovery ratio of about 53%.

(6) For mine refuge chambers with an initial surrounding rock temperature of 32℃ or more, the economy of the mine compressed air-ice storage-surrounding rock scheme will reflect after the surrounding rock is cooled to equivalent 32℃ or below.

Declaration of competing interest

The authors declare that they have no known competing financial interests or personal relationships that could have appeared to influence the work reported in this paper.

Acknowledgments

The authors would like to thank the financial support from the National Natural Science Foundation of China (52168013), the Natural Science Foundation of Guizhou Province (ZK[2022]151) and the State Key Laboratory of Gas Disaster Detecting, Preventing and Emergency Controlling Open-fund Project (2021SKLKF10).

References

[1] K. Guerra, R. Gutiérrez-Alvarez, O.J. Guerra, P. Haro, Opportunities for low-carbon generation and storage technologies to decarbonise the future power system, Appl. Energy 336 (2023) 120828, https://doi.org/10.1016/j.apenergy.2023.120828.

[2] X. Zheng, Y. Zhou, A three-dimensional unsteady numerical model on a novel aerogel-based pv/t-pcm system with dynamic heat-transfer mechanism and solar energy harvesting analysis, Appl. Energy 338 (2023) 120899, https://doi.org/10.1016/j.apenergy.2023.120899.

[3] M.T. Ameen, Z. Ma, A. Smallbone, R. Norman, A.P. Roskilly, Experimental study and analysis of a novel layered packed-bed for thermal energy storage applications: a proof of concept, Energy Conv. Manag. 277 (2023) 116648, https://doi.org/10.1016/j.enconman.2022.116648.

[4] C. Semeraro, A.G. Olabi, H. Aljaghoub, A.H. Alami, M. Al Radi, M. Dassisti, M.A. Abdelkareem, Digital twin

application in energy storage: trends and challenges, J. Energy Storage 58 (2023) 106347, https://doi.org/10.1016/j.est.2022.106347.

[5] O. Mahian, M. Javidmehr, A. Kasaeian, S. Mohasseb, M. Panahi, Optimal sizing and performance assessment of a hybrid combined heat and power system with energy storage for residential buildings, Energy Conv. Manag. 211 (2020) 112751, https://doi.org/10.1016/j.enconman.2020.112751.

[6] M. Deymi-Dashtebayaz, I.V. Baranov, A. Nikitin, V. Davoodi, A. Sulin, M. Norani, V. Nikitina, An investigation of a hybrid wind-solar integrated energy system with heat and power energy storage system in a near-zero energy building-a dynamic study, Energy Conv. Manag. 269 (2022) 116085, https://doi.org/10.1016/j.enconman.2022.116085.

[7] L. Hu, Y. Liu, D. Wang, X. Luo, H. Liu, Feasibility analysis and feature comparison of cold thermal energy storage for off-grid pv air-conditioned buildings in the tropics, Energy Conv. Manag. 254 (2022) 115176, https://doi.org/10.1016/j.enconman.2021.115176.

[8] M. Barthwal, A. Dhar, S. Powar, The techno-economic and environmental analysis of genetic algorithm (ga) optimized cold thermal energy storage (ctes) for air-conditioning applications, Appl. Energy 283 (2021) 116253, https://doi.org/10.1016/j.apenergy.2020.116253.

[9] J. Cho, J. Woo, Development and experimental study of an independent row-based cooling system for improving thermal performance of a data center, Appl. Therm. Eng. 169 (2020) 114857, https://doi.org/10.1016/j.applthermaleng.2019.114857.

[10] B.B. Kanbur, C. Wu, S. Fan, F. Duan, System-level experimental investigations of the direct immersion cooling data center units with thermodynamic and thermoeconomic assessments, Energy 217 (2021) 119373, https://doi.org/10.1016/j.energy.2020.119373.

[11] C. Zeng, Y. Yuan, F. Haghighat, K. Panchabikesan, X. Cao, L. Yang, Z. Leng, Thermo-economic analysis of geothermal heat pump system integrated with multi-modular water-phase change material tanks for underground space cooling applications, J. Energy Storage 45 (2022) 103726, https://doi.org/10.1016/j.est.2021.103726.

[12] X. Gao, Y. Xiao, P. Gao, Thermal potential improvement of an earth-air heat exchanger (eahe) by employing backfilling for deep underground emergency ventilation, Energy 250 (2022) 123783, https://doi.org/10.1016/j.energy.2022.123783.

[13] K.A. Margolis, C.Y.K. Westerman, K.M. Kowalski-Trakofler, Underground mine refuge chamber expectations training: program development and evaluation, Saf. Sci. 49 (3) (2011) 522-530, https://doi.org/10.1016/j.ssci.2010.12.008.

[14] C. Mejías, D. Jiménez, A. Muñoz, L. Reyes-Bozo, Clinical response of 20 people in a mining refuge: study and analysis of functional parameters, Saf. Sci. 63 (2014) 204-210, https://doi.org/10.1016/j.ssci.2013.11.011.

[15] Z. Zhang, Y. Yuan, K. Wang, X. Gao, X. Cao, Experimental investigation on influencing factors of air curtain systems barrier efficiency for mine refuge chamber, Process Saf. Environ. Protect. 102 (2016) 534-546, https://doi.org/10.1016/j.psep.2016.05.008.

[16] E. Paul Meisburger, D. Iryanto, D. Quinn, A. Widyastutie, A. Mone, Design and construction of high capacity fixed refuge chambers at pt freeport indonesia's underground operations, in: X. Chang (Ed.), Springer Singapore, Singapore, 2019, pp. 850-859. https://doi.org/10.1007/978-981-13-1420-9_73

[17] K.E. Karadeniz, S. Nowak, D. Guner, T. Sherizadeh, Evaluation on underground refuge alternatives and explosion survivability: a review, Mining, Metallurgy & Exploration 39 (6) (2022) 2311-2331, https://doi.org/10.1007/s42461-022-00682-1.

[18] Z. Shao, Y.C. Yang, M. Kumral, Optimal refuge chamber position in underground mines based on tree network, Int. J. Inj. Control Saf. Promot. 30 (2) (2023) 294-309, https://doi.org/10.1080/17457300.2022.2164311.

[19] Y. Li, Y. Yuan, C. Li, X. Han, X. Zhang, Human responses to high air temperature, relative humidity and carbon dioxide concentration in underground refuge chamber, Build. Environ. 131 (2018) 53-62, https://doi.org/10.1016/j.buildenv.2017.12.038.

[20] D.Y.M.K. L. Yan, Validation of temperature and humidity thermal model of 23-person tent-type refuge alternative. Society for mining, Metallurgy, and Exploration (340) (2016) 225-231, http://dx.chinadoi.cn/http://dx.doi.org/10.19150/me.6759.

[21] B. Yang, H. Yao, P. Yang, Y. Guo, F. Wang, C. Yang, A. Li, L. Che, Effects of thermal and acoustic environments on workers' psychological and physiological stress in deep underground spaces, Build. Environ. 212 (2022) 108830, https://doi.org/10.1016/j.buildenv.2022.108830.

[22] R. Qiao, X. Li, S. Gao, X. Ma, Improvement of thermal comfort for underground space: data enhancement using variational autoencoder, Build. Environ. 207 (2022) 108457, https://doi.org/10.1016/j.buildenv.2021.108457.

[23] D.S.Y.E. T. Bernard, estimation of metabolic heat input for refuge alternative thermal testing and simulation, Min. Eng. (70) (2018) 50-54, https://doi.org/10.19150/me.8429.

[24] Z. Zhang, T. Jin, H. Wu, R. Day, X. Gao, K. Wang, R. Mao, Experimental investigation on environmental control of a 50-person mine refuge chamber, Build. Environ. 210 (2022) 108667, https://doi.org/10.1016/j.buildenv.2021.108667.

[25] Z. Zhang, H. Wu, K. Wang, R. Day, Y. Yuan, Thermal performance of a mine refuge chamber with human body heat sources under ventilation, Appl. Therm. Eng. 162 (2019) 114243, https://doi.org/10.1016/j.applthermaleng.2019.114243.

[26] A.E. Halim, J.F. Brune, Do refuge chambers represent a good strategy to manage emergencies in underground coal mines? Mining, Metallurgy & Exploration 36 (6) (2019) 1191-1199, https://doi.org/10.1007/s42461-019-0100-8.

[27] X. Gao, Z. Zhang, Y. Xiao, Modelling and thermo-hygrometric performance study of an underground chamber with a long vertical earth-air heat exchanger system, Appl. Therm. Eng. 180 (2020) 115773, https://doi.org/10.1016/j.applthermaleng.2020.115773.

[28] Z. Zhang, H. Wu, K. Wang, R. Day, Y. Yuan, Air quality control in mine refuge chamber with ventilation through pressure air pipeline, Process Saf. Environ. Protect. 135 (2020) 46-58, https://doi.org/10.1016/j.psep.2019.12.014.

[29] H. Shao, S. Jiang, W. Tao, Z. Wu, W. Zhang, K. Wang, Theoretical and numerical simulation of critical gas supply of refuge chamber, Int. J. Min. Sci. Technol. 26 (3) (2016) 389-393, https://doi.org/10.1016/j.ijmst.2016.02.004.

[30] D.S. Yantek, L. Yan, N.W. Damiano, M.A. Reyes, J.R. Srednicki, A test method for evaluating the thermal environment of underground coal mine refuge alternatives, Int. J. Min. Sci. Technol. 29 (3) (2019) 343-355, https://doi.org/10.1016/j.ijmst.2019.01.004.

[31] D.S. Yantek, L. Yan, P.T. Bissert, M.D. Klein, Effects of mine strata thermal behavior and mine initial temperatures on mobile refuge alternative temperature, Min. Eng. 4 (69) (2017) 41-48, https://doi.org/10.19150/me.7393.

[32] L. Yan, D.S. Yantek, M.A. Reyes, Underground mine air and strata temperature change due to the use of refuge alternatives, Mining, Metallurgy & Exploration 37 (2) (2020) 773-781, https://doi.org/10.1007/s42461-019-00153-0.

[33] B.C.C.V. Friedenstein, Simulating operational improvements on mine compressed air systems, The South African Journal of Industrial Engineering 3 (29) (2018) 69-81, https://doi.org/10.7166/29-3-2049.

[34] S. Wang, L. Jin, Z. Han, Y. Li, S. Ou, N. Gao, Z. Huang, Discharging performance of a forced-circulation ice thermal storage system for a permanent refuge chamber in an underground mine, Appl. Therm. Eng. 110 (2017) 703-709, https://doi.org/10.1016/j.applthermaleng.2016.08.192.

[35] Y. Jia, Y. Liu, S. Sun, H. Li, L. Jiao, Refrigerating characteristics of ice storage capsule for temperature control of coal mine refuge chamber, Appl. Therm. Eng. 75 (2015) 756-762, https://doi.org/10.1016/j.applthermaleng.2014.10.036.

[36] X. Xu, S. You, X. Zheng, H. Zhang, S. Liu, Cooling performance of encapsulated ice plates used for the underground refuge chamber, Appl. Therm. Eng. 112 (2017) 259-272, https://doi.org/10.1016/j.applthermaleng.2016.10.072.

[37] Y. Du, W. Gai, L. Jin, W. Sheng, Thermal comfort model analysis and optimization performance evaluation of a multifunctional ice storage air conditioning system in a confined mine refuge chamber, Energy 141 (2017) 964-974, https://doi.org/10.1016/j.energy.2017.09.123.

[38] X. Gao, Y. Yuan, X. Cao, H. Wu, X. Zhao, D. Yan, Coupled cooling method and application of latent heat thermal energy storage combined with pre-cooling of envelope: temperature control using phase-change chair, Sust. Cities Soc. 42 (2018) 38-51, https://doi.org/10.1016/j.scs.2018.06.032.

[39] X. Gao, Z. Zhang, Y. Yuan, X. Cao, C. Zeng, D. Yan, Coupled cooling method for multiple latent heat thermal storage devices combined with pre-cooling of envelope: model development and operation optimization, Energy 159 (2018) 508-524, https://doi.org/10.1016/j.energy.2018.06.151.

[40] Y. Junling, Y. Luwei, W. Juan, M. Yuezheng, Z. Zhentao, Study on open-cycle carbon dioxide refrigerator for movable mine refuge chamber, Appl. Therm. Eng. 52 (2) (2013) 304-312, https://doi.org/10.1016/j.applthermaleng.2012.12.014.

[41] L. Yan, D. Yantek, M. Reyes, B. Whisner, J. Bickson, J. Srednicki, N. Damiano, E. Bauer, Cryogenic air supply for cooling built-in-place refuge alternatives in hot mine, Mining, Metallurgy & Exploration 37 (3) (2020) 861-871, https://doi.org/10.1007/s42461-020-00194-w.

[42] Y. Yuan, X. Gao, H. Wu, Z. Zhang, X. Cao, L. Sun, N. Yu, Coupled cooling method and application of latent heat thermal energy storage combined with pre-cooling of envelope: method and model development, Energy 119 (2017) 817-833, https://doi.org/10.1016/j.energy.2016.11.058.

[43] Z. Zhang, W. Guo, X. Gao, H. Wu, R. Mao, Investigation on temperature control based on cooled mine compressed air for mine refuge chamber with high-temperature surrounding rock, Int. J. Therm. Sci. 187 (2023) 108201, https://doi.org/10.1016/j.ijthermalsci.2023.108201.

[44] M. Khabbaz, B. Benhamou, K. Limam, P. Hollmuller, H. Hamdi, A. Bennouna, Experimental and numerical study of an earth-to-air heat exchanger for air cooling in a residential building in hot semi-arid climate, Energy Build. 125 (2016) 109-121, https://doi.org/10.1016/j.enbuild.2016.04.071.

[45] X. Guo, H. Wei, X. He, J. Du, D. Yang, Experimental evaluation of an earth–to–air heat exchanger and air source

heat pump hybrid indoor air conditioning system, Energy Build. 256 (2022) 111752, https://doi.org/10.1016/j.enbuild.2021.111752.

[46] G.F. Frate, L. Ferrari, P. Sdringola, U. Desideri, A. Sciacovelli, Thermally integrated pumped thermal energy storage for multi-energy districts: integrated modelling, assessment and comparison with batteries, J. Energy Storage 61 (2023) 106734, https://doi.org/10.1016/j.est.2023.106734.

[47] M.T. Ameen, Z. Ma, A. Smallbone, R. Norman, A.P. Roskilly, Experimental study and analysis of a novel layered packed-bed for thermal energy storage applications: a proof of concept, Energy Conv. Manag. 277 (2023) 116648, https://doi.org/10.1016/j.enconman.2022.116648.

[48] K. Knobloch, Y. Muhammad, M.S. Costa, F.M. Moscoso, C. Bahl, O. Alm, K. Engelbrecht, A partially underground rock bed thermal energy storage with a novel air flow configuration, Appl. Energy 315 (2022) 118931, https://doi.org/10.1016/j.apenergy.2022.118931.

[49] K. Knobloch, T. Ulrich, C. Bahl, K. Engelbrecht, Degradation of a rock bed thermal energy storage system, Appl. Therm. Eng. 214 (2022) 118823, https://doi.org/10.1016/j.applthermaleng.2022.118823.

[50] N.B. Desai, M.E. Mondejar, F. Haglind, Techno-economic analysis of two-tank and packed-bed rock thermal energy storages for foil-based concentrating solar collector driven cogeneration plants, Renew. Energy 186 (2022) 814-830, https://doi.org/10.1016/j.renene.2022.01.043.

[51] X. Bai, Z. Tang, A numerical study of rock bed seasonal thermal storage used for mine ventilation, Sustain. Energy Technol. Assess. 50 (2022) 101867, https://doi.org/10.1016/j.seta.2021.101867.

[52] J.C.W.S. Shuai Zhu, Using seasonal temperature difference in underground surrounding rocks to cooling ventilation airflow: a conceptual model and simulation study, Energy Sci. Eng. 8 (10) (2020) 3457-3475, https://doi.org/doi.org/10.1002/ese3.619.

[53] X. Zhang, B. Bu, L. Liu, T. Cao, Y. Ke, Q. Du, Z. Han, Y. Duan, Study on temperature drop and cooling effect of cold wall for backfill body with embedded cold fluid tube, Int. J. Therm. Sci. 184 (2023) 107904, https://doi.org/10.1016/j.ijthermalsci.2022.107904.

[54] W. Guo, Z. Zhang, H. Wu, L. Ge, X. Liang, R. Mao, Experimental study on cooling and dehumidification performance of an ice storage air conditioner used in underground refuge chamber, Int. Commun. Heat Mass Transf. 146 (2023) 106930, https://doi.org/10.1016/j.icheatmasstransfer.2023.106930.

[55] Z. Zhang, W. Guo, H. Wu, L. Ge, Xing Liang, R. Mao, Thermal performance of an ice storage device for cooling compressed mine air in high-temperature mine refuge chambers, Appl. Therm. Eng. 233 (2023) 121101, https://doi.org/10.1016/j.applthermaleng.2023.121101.

[56] X. Gao, Y. Yuan, H. Wu, X. Cao, X. Zhao, Coupled cooling method and application of latent heat thermal energy storage combined with pre-cooling of envelope: optimization of pre-cooling with intermittent mode, Sust. Cities Soc. 38 (2018) 370-381, https://doi.org/10.1016/j.scs.2018.01.014.

[57] Q. Cao, M. Liu, X. Li, C. Lin, D. Wei, S. Ji, T.T. Zhang, Q. Chen, Influencing factors in the simulation of airflow and particle transportation in aircraft cabins by cfd, Build. Environ. 207 (2022) 108413, https://doi.org/10.1016/j.buildenv.2021.108413.

[58] J. Lin, Y. Kong, L. Zhong, Optimization of environment control system for narrow sleeping space in underground shelters, Energy Build. 263 (2022) 112043, https://doi.org/10.1016/j.enbuild.2022.112043.

[59] T. Wu, C. Lei, On numerical modelling of conjugate turbulent natural convection and radiation in a differentially heated cavity, Int. J. Heat Mass Transf. 91 (2015) 454-466, https://doi.org/10.1016/j.ijheatmasstransfer.2015.07.113.

[60] M. Boulet, B. Marcos, M. Dostie, C. Moresoli, Cfd modeling of heat transfer and flow field in a bakery pilot oven, J. Food Eng. 97 (3) (2010) 393-402,https://doi.org/10.1016/j.jfoodeng.2009.10.034.

[61] Z. Zhang, R. Day, K. Wang, H. Wu, Y. Yuan, Thermal performance analysis of an underground closed chamber with human body heat sources under natural convection, Appl. Therm. Eng. 145 (2018) 453-463, https://doi.org/10.1016/j.applthermaleng.2018.09.068.

Highlights

1. An improved temperature control scheme was proposed for mine refuge chambers.
2. Ventilation with a rate of 300 m^3/h can be cooled to 20°C from 35°C by ice storage unit.
3. The scheme is applicable to mine refuge chambers with an initial surrounding rock temperature of 35℃ or more.
4. During pre-cooling, temperature gradient of surrounding rock is related to ventilation but not to initial surrounding rock temperature.
5. The scheme is more economical when the surrounding rock temperature is cooled to below 32°C

Declaration of Interest Statement

We declare that we have no financial and personal relationships with other people or organizations that can inappropriately influence our work, there is no professional or other personal interest of any nature or kind in any product, service and/or company that could be construed as influencing the position presented in the manuscript entitled, '*Performance analysis of an improved temperature control scheme with cold stored in surrounding rock for underground refuge chamber*'.

Performance analysis of an improved temperature control scheme with cold stored in surrounding rock for underground refuge chamber

Zujing Zhang[a,b*], Weishuang Guo[a], Ruiyong Mao[a], Liang Ge[b], Xing Liang[c], Hongwei Wu[d**]

[a] College of Civil Engineering, Guizhou Provincial Key Laboratory of Rock and Soil Mechanics and Engineering Safety, Guizhou University, Guiyang, 550025, China

[b] State Key Laboratory of Gas Disaster Detecting, Preventing and Emergency Controlling, Chongqing Research Institute of China coal Technology and Engineering Group Co. Ltd., Chongqing, 400037, China

[c] School of Computer Science and Mathematics, Kingston University London, KT1 2EE, United Kingdom

[d] School of Physic, Engineering and computer science, University of Hertfordshire, Hatfield, AL10 9AB, United Kingdom

[*]Corresponding author: email: zjzhang3@gzu.edu.cn.

[**]Corresponding author: email: h.wu6@herts.ac.uk.

Abstract: This article proposed an improved temperature control scheme that combines mine compressed air, ice storage and surrounding rock, for mine refuge chambers. The feasibility of cooling mine compressed air via an ice storage unit was experimentally demonstrated, and the performance and temperature control performance of low-temperature mine compressed air on pre-cooling of surrounding rock were studied by numerical simulation. Results showed that: (i) The ice storage unit cools ventilation with a volume flow rate of 300 m^3/h could be cooled to 20℃ from 35℃. For mine refuge chambers with an initial surrounding rock temperature of 35℃, the ambient temperature could be kept below 35℃ within 96 h, after pre-cooling the surrounding rock through continuously ventilating for 30 days at normal time. (ii) During pre-cooling, the surrounding rock temperature drops exponentially over time, and the temperature gradient decreases with ventilation rate and ventilation temperature, but has little to do with initial surrounding rock temperature. However the temperature of pre-cooled surrounding rock changes little when the ratio of ventilation time to non-ventilation time is 53:100 for mine refuge chambers with an initial surrounding rock temperature of 35°C. (iii) For mine refuge chambers with an initial surrounding rock temperature of 32℃ or higher, the economy of the mine compressed air-ice storage-surrounding rock scheme will be reflected when the equivalent surrounding rock is 32℃ or lower.

Key words: Mine refuge chamber; Temperature control; Mine compressed air; Cold storage; Surrounding rock.

Nomenclature

C_p	Specific heat capacity of air, kJ/(kg·k)	***Greek symbols***	
C_1, C_2	Model parameters	ρ	Air density, kg/m^3
$C_{1\varepsilon}$, $C_{3\varepsilon}$	Model parameters	τ	Ventilating time, h
e	Natural base, 2.7182818284	ε	Turbulent energy dissipation, J/(kg·s)
G	Ventilation rate for MRC, m^3/h	β	Coefficient of thermal expansion, 1/K
g_i	Acceleration component of gravity in the i directions, m/s^2	λ	Air thermal conductivity, W/(m·K)
n	Number of IS units	μ	Dynamic viscosity, Pa·s
q	Cold capacity of an ice storage unit, kJ	μ_τ	Turbulent viscosity, Pa·s
Q	Total heat rate in a MRC, W	σ_k	Prandt1 number
Q_m	Cold capacity for a MRC, kJ	σ_ε	Prandt1 number
T_a	Air temperature in MRC, °C	***Acronyms***	
T_{eisr}	Equivalent ISRT, °C	AT	Ambient temperature
T_{isr}	Initial surrounding rock temperature, °C	HR	Heat rate
T_{mca}	Mine compressed air temperature, °C	ISRT	Initial surrounding rock temperature
T_v	Ventilation temperature in MRC, °C	IS	Ice storage
Subscripts		MCA	Mine compressed air
G_b	Generation of turbulence kinetic energy due to buoyancy, J/(s m^3)	MCA-ISAC	IS air conditioner for cooling MCA
G_k	Generation of turbulence kinetic energy due to the mean velocity gradients, J/(s m^3)	MRC	Mine refuge chamber
h	Coefficient in K expression	PCM	Phase change material
i	Coefficient in K expression	SRT	Surrounding rock temperature
j	Coefficient in K expression	SR	Surrounding rock
k	turbulent kinetic energy (J/kg)	VR	Ventilation rate
t	Time s	VT	Ventilation temperature

1 Introduction

Energy storage technology has attracted much attention with rapid development and application of renewable energy [1]. Thermal energy storage systems, including latent heat storage such as phase change material (PCM) device and sensible heat storage such as rock-bed thermal storage system, play an important role in the process of energy storage and application [2,3]. In the field of artificial

environmental control, thermal storage systems can not only promote the application of intermittent or unstable renewable energy such as solar energy, geothermal energy, wind energy, etc., in living and office buildings [4-6], but also make it possible to regulate the artificial environment of some living spaces with air conditioning demand but limited by electrical power such as buildings in remote areas [7,8], data centers [9,10], and underground facilities [11,12].

The mine refuge chamber (MRC) as one of the main safety facilities applied in many countries such as the United States [13], Chile [14], China [15], and Indonesia [16], etc., for underground mines to protect workers against mine disasters. MRC needs to take temperature control measure to keep the ambient temperature (AT) at an acceptable level within 96 h [17-22], and balancing the heat generated from human metabolism and equipment operation as well as high-temperature surrounding rock (SR) [23-25]. During the period of taking shelter, connected to the ground only through a protected air supply pipeline linked to the underground mine compressed air (MCA) system or a vertical borehole from the surface air compressor [26,27]. The rated ventilation rate (VR) for the MCA system is 0.1 m^3/min per capita which needs cover all people in the underground mine, and the rated VR for a MRC is 0.3 m^3/min per capita [28]. However, in order to balance the heat generated by occupants sitting in the MRC, the ventilation temperature (VT) needs to below 15°C when the VR is 0.3 m^3/min per capita, in the case of without considering the heat dissipation influence of the SR [29]. As is normally the case, the SR plays a very important role in determining the temperature control of MRCs [30-32]. When the initial surrounding rock temperature (ISRT) is over 27°C, the MCA with a VR of 0.3 m^3/min per capita cannot maintain the AT less than 35°C within 96 h [25]. Consider increased ventilation costs for MCA systems or the cost of the surface borehole, the economics of the original MCA in cooling the MRC will be significantly reduced for MRCs with high ISRTs [33].

Over the past decade, based on the cold energy storage, several cooling technologies including ice storage (IS) cooling [34-37], PCM cooling [38,39], liquid CO_2 cooling [40] and liquid-air cooling systems [41] have been developed for MRCs. Among them, liquid CO_2 cooling technology can only be used normally in environments where the temperature is below 32°C [42], and the economics of the PCM cooling technology can only be obtained in a MRC with a lower ISRT [38,39]. Although the liquid-air cooling technology is suitable for different temperature environments, its cost is far higher than that of the other technologies [41]. Zhang et al. [43] proposed a novel control temperature scheme that directly connecting the MCA to an IS unit, but it is only applicable to MRCs with an ISRT below 32 °C. Due to SR has good thermal conductivity, high density latent heat storage capacity and is inexpensive, thermal energy storage systems taking SR as heat carrier have attracted more attention in recent years, such as earth-to-air heat exchanger [44,45] and thermal energy storage battery [46] for ground buildings, rock-bed thermal storage systems[47-50]. Bai et al. [51] developed a seasonal heat storage scheme for rock formations, which saves energy for remote mine ventilation through numerical simulation analysis. Zhu et al. [52] used Abaqus software for numerical analysis to proposed a mathematical model of heat regulation and energy storage of SR in a mine tunnel and demonstrated the cooling storage capacity of the SR heat regulation circle. Zhang et al. [53] used

Ansys-Fluent software to proposed a radiation cooling measure by cold the rock wall via heat transfer tubes for high-temperature the underground mine working face.

Nowadays, in terms of temperature control in MRC, attention is being paid to the cold energy stored in SR. Yuan et al. [42] proposed a novel cooling scheme combining cold storage in SR and PCM for MRCs and carried out a semi-analysis to analyze the refrigeration performance of SR. The temperature of the SR and air within the MRC will be pre-cooled at normal times by an available cold source to store a certain amount of cooling and a small amount of PCM. Guo et al. [54,55] developed an ice storage device combining MCA with mixed air supply cooling high temperature MRC, and through experiments and numerical simulations to analyzed the cooling performance of the ice storage device. The results show that during the 96h evacuation period, the ice storage device can control the ambient temperature of MRC with an SRT of 32°C within 35°C. Gao et al. [12,27] combined experimental and numerical studies on the performance of a ground-air heat exchanger for controlling the ambient temperature of MRC. Their result showed that for a MRC buried at a depth of 400 m and with an ISRT of 28.5 °C, the earth-to-air system could maintain the AT below 30 °C within 96 h at a VR of 0.3 m^3/min per capita, but it is not suitable for MRCs buried at depths of more than 400 m. Gao et al. [56] proposed an interchanging continuous and intermittent cold storage strategy for pre-cooling the SR in a MRC, this strategy reduces an annual cold storage energy consumption by 68-78%, compared with the continuous mode.

It is aforementioned from previous studies that for MRCs with high ISRTs, it is difficult to control the indoor AT by the MCA alone, thus cold storage is an effective supplement. This study develops an improved composite temperature control scheme combining the safe and economical MCA-ISAC and SR cold storage with the existing MCA for MRCs with high ISRTs. A set of MCA-ISAC used was fabricated and tested to prove the feasibility of cooling the MCA. Moreover, the thermal performance of cold storage in the SR and the temperature control performance of the improved scheme in MRC were studied in a systematic manner. This study solves the temperature control problem of MRCs with high ISRT, and provides theoretical guidance for the multi-coupled temperature control technology of MRC.

2 Methodology

2.1 Principle of the MCA-IS-SR system

In the current work, an improved temperature control scheme combining MCA with cold energy stored by IS and SR (Abbreviated as MCA-IS-SR) is proposed for MRCs with ISRTs higher than 32°C, as shown in Fig. 1. The MCA pipeline entering the MRC is directly linked to an IS unit, the temperature of the MCA will be cooled through the heat exchange with heat exchanger tubes of the MCA-ISAC. During non-refuge period, the IS unit can operate normally, enough ice will be stored in the MCA-ISAC by running the refrigeration compressor periodically, and the SR temperature (SRT) will be pre-cooled by the cooled MCA to store a certain amount of cold energy. During the refuge period, in case of underground power outage, the temperature control requirement is achieved through the cooled MCA and the pre-cooled SR. The advantage of the improved scheme is that it not only retains the advantages of IS technology and makes full use of the MCA in the absence of underground

electrical power, but also uses the free SR with high potential in energy storage as a cold storage carrier.

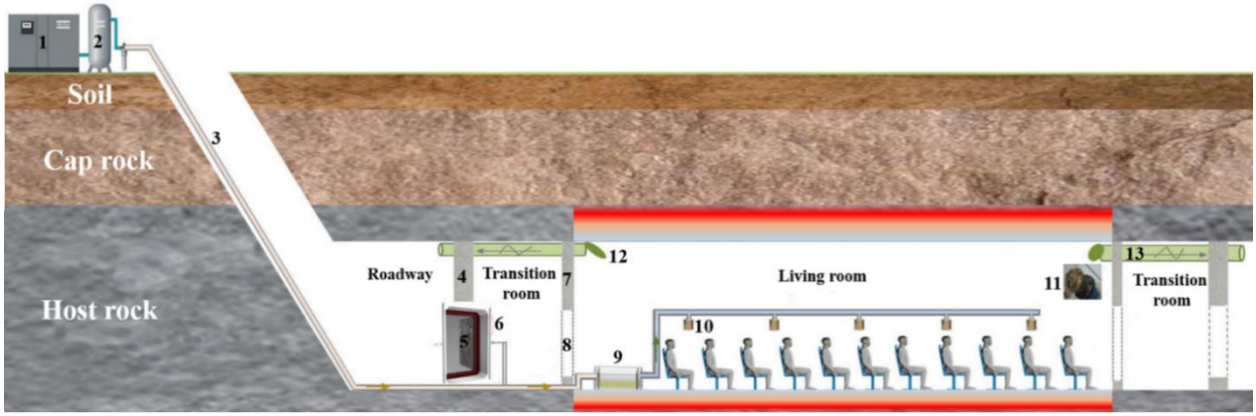

1 - Air compressor, 2 - Air storage tank, 3 - pipeline, 4 - Explosion-protection wall, 5- Protective airtight door, 6 - Air curtain, 7 - Seal wall, 8 - Airtight door, 9 - MCA-ISAC, 10 - Silence air inlet, 11 - One-way exhaust valve, 12 - Air outlet, 13 - Exhaust outlet.

Fig. 1 Principle of the MCA-IS-SR system for high-temperature MRCs.

2.2 Experimental setup

2.2.1 Experimental environment and principle

To test the ability of the MCA-ISAC unit on cooling the MCA, a cuboid MCA-ISAC unit with length, width and height are 1.3 m × 0.7 m × 1.2 m was designed. It is made of 2 mm-thick stainless steel plates and has stress-bearing parts welded inside. The outer wall of the tank is covered with a 30 mm-thick polyurethane insulation material to reduce the heat loss. Circular air inlet and outlet with a diameter of 0.1 m and the air buffer of 0.8 m × 0.5 m × 0.1 m are set at both ends. Between the two air buffers, 18 stainless steel heat exchanger tubes with a length of 1.1 m, an inner diameter of 30 mm and a wall thickness of 2.5 mm are evenly arranged at a horizontal distance of 0.15 m and a height distance of 0.2 m. The copper coiled condenser is submerged inside the tank of the MCA-ISAC unit, then connected to a compression freezer (AOSZGA-040) with a cooling capacity of 5 kW. This can freeze the ice to -30°C and maintain a certain cooling capacity until the temperature of the water in the tank exceeds 20°C. A frequency conversion fan is placed in an artificial environment room with length, width and height are 3.6 m × 3.1 m × 3.0 m, in which the air temperature can be controlled at a relatively stable value in the range of 20 ~ 60 ℃with the assistance of a ventilation heat exchange system. The fan can control the pipeline air speed in the range of 0 ~ 30 m/s, the fan is connected to the air inlet of the IS unit outside the artificial environment room by a steel pipe with a diameter of 0.1 m. The hot air in the artificial environment room is sent to the heat exchange tube of the MCA-ISAC unit through the fan airflow guidance, and after cooling, it flows into the external environment form the air outlet. The experimental principle and experimental environment are shown in Fig. 2 (a) and (b), respectively.

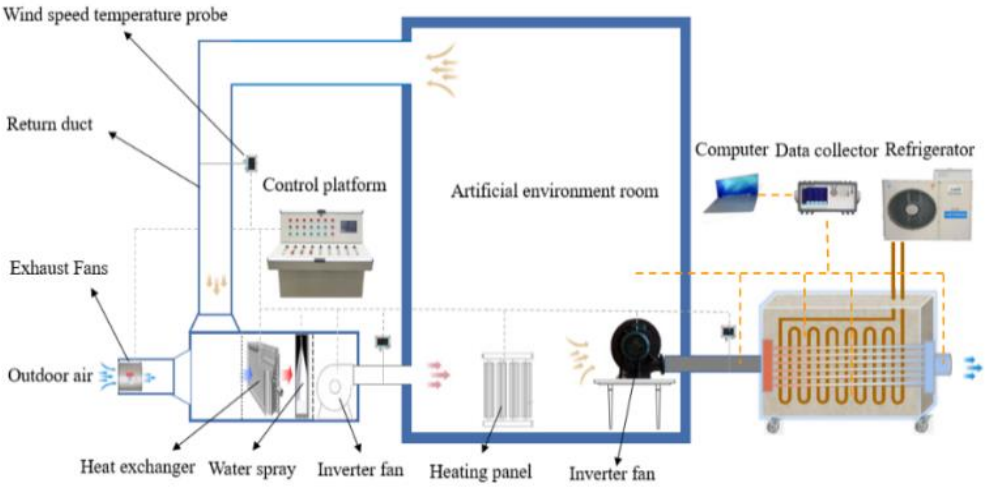

(a) Experimental principle

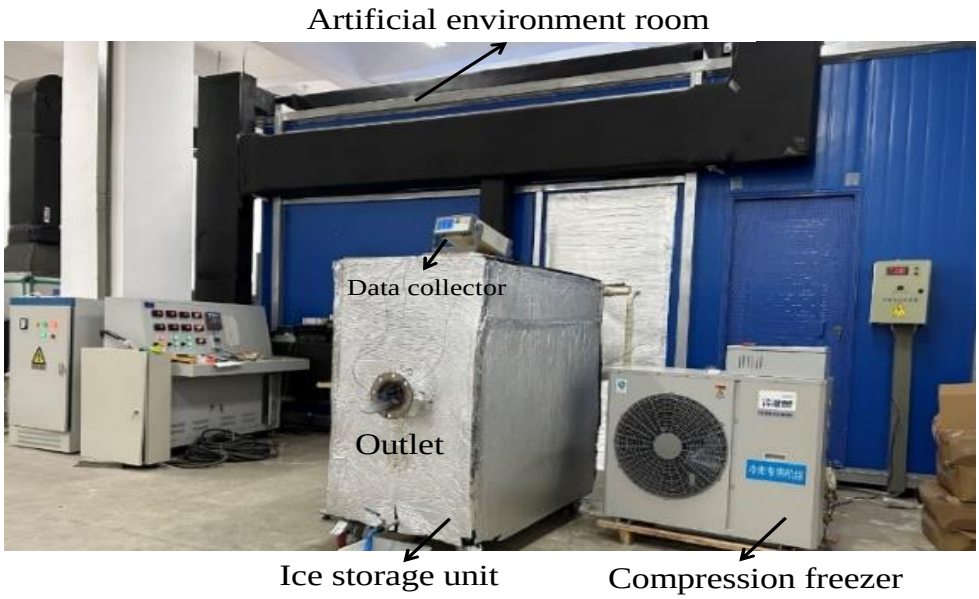

(b) Experimental environment

Fig. 2 Experimental principle and environment for the MCA-ISAC unit.

2.2.3 Data collection

To test the air speed and temperature at the air inlet, a plug-in pipe measuring instrument that can measure the air speed and temperature is fixed on the inlet air supply pipe. In the current work, the air speed is in the range of 0~20 m/s with an accuracy of 0.1 m/s, while the temperature ranges from 0°C to 60°C with an accuracy of 0.1°C. In order to make the inlet air temperature more accurate, a temperature monitoring point was allocated to the inlet air supply pipe. There are 3 temperature monitoring point located at the air outlet to measure the outlet air temperature, and a portable anemometer is used to measure the air speed at the air outlet. In the IS tank, 6 temperature monitoring points are arranged at the level of 0.3 m and 0.9 m above the bottom, and 8 temperature monitoring points are arranged at the 0.6 m level. The K-type thermocouples with a measurement range of 0~200°C and an accuracy of 0.01°C are used to measure the temperature. The measurement data will be automatically recorded per minute and saved every 5 minutes by a data acquisition.

2.2.4 Design of experimental cases

During the refuge period, the heat dissipation rate is about 120 W per capita [24]. The tank has

a volume of about 1 m^3, its cold storage capacity is around 4.14×10^5 kJ including sensible heat of 1.06×10^5 kJ and latent heat of 3.08×10^5 kJ. Assuming that the air supply rate is the rated value of 0.3 m^3/min per capita and the indoor AT is maintained at 35 °C, the cold capacity stored by the MCA-ISAC unit can balance the heat capacity of about 10 people within 96 h without considering heat exchange between SR and air. Practically, the heat exchange between the air and SR can have an important effect on the indoor air temperature control. In a MRC with an ISRT of 30°C, according to the AT prediction method in the ref. [43], the MCA cooled by an MCA-ISAC unit will meet the temperature control requirement of about 17 people. The air supply rates for 10 and 17 people are 3 m^3/min and 4.5 m^3/min, respectively, and their corresponding speeds at the air inlet of the IS unit are 6.37 m/s and 10.82 m/s. Table 1 lists the parameters of the current experimental cases.

Table. 1 Parameters of experimental cases

Case	Inlet air speed (m/s)	Inlet air temperature (°C)	Initial temperature of tank (°C)	Time (h)
1	7	35	-25	96
2	11	30	-28	96

2.2.5 Experimental procedure

The main experimental steps are as follows:

(1) Fix the temperature sensor at the corresponding points in the MCA-ISAC tank, then turn on the temperature data collector to ensure the reliability of data acquisition.

(2) Add water to the tank until it reaches the water level at 0.85 m high.

(3) Run the refrigeration unit until all measuring point temperatures are below -25°C.

(4) Turn on the heating equipment for the artificial environment control room, and maintain the fresh air entering the room at approximately 35°C.

(5) Turn on the frequency fan to make the hot air enter heat exchange tubes of the MCA-ISAC.

(6) Adjust the air speed in the air duct through the fan inverter to 7 m/s.

(7) Stop the test after continuous ventilation for more than 96 h.

(8) Repeat the above steps to complete experimental case 2.

(9) Record and analyse the experimental data.

2.3 Numerical methodologies

2.3.1 Grid model

A grid model of a 50-person MRC will be established, referring to the internal structure of the MRC laboratory in the ref. [43]. The internal size of the MRC is 20 m in length, 4 m in width and 3 m in height, the thickness of the SR is 8 m. Fifty human bodies with a surface area of 2 m^2 are divided into 4 rows in the living room. At above the ground 1.8 m, there are 5 air inlets with a diameter of 0.075 m and a distance between two adjacent inlets of 3.5 m located on each side. As shown in Fig. 3 (a), at above the floor 2.7 m, there is an air outlet with a diameter of 0.225 m located on each end. The mesh of the computational model of the MRC was generated by ANSYS ICEM and the unstructured mesh was adopted. Taking the grid independence study into account, an unstructured grid model with a mesh number of 3.49 million and a minimum orthogonal quality is selected for the

following numerical analysis, see in Fig. 3 (b).

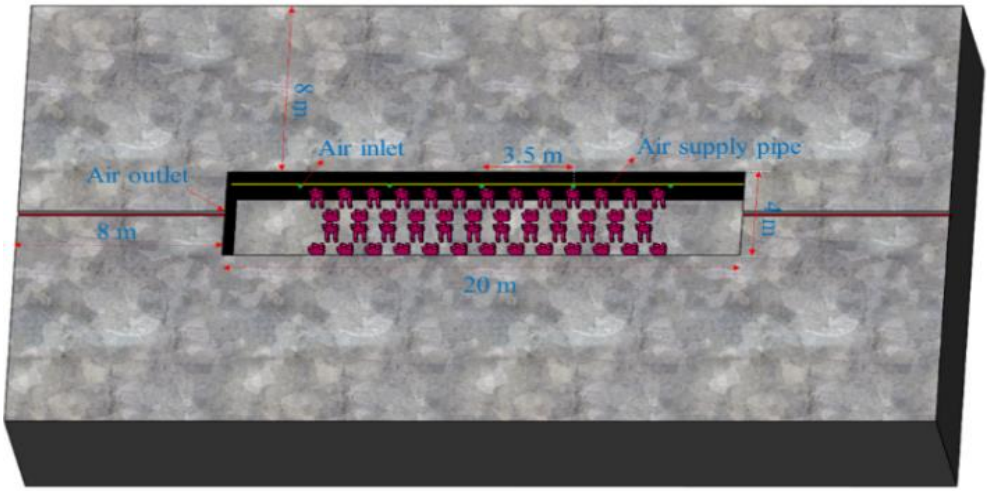

(a) **Geometry model**

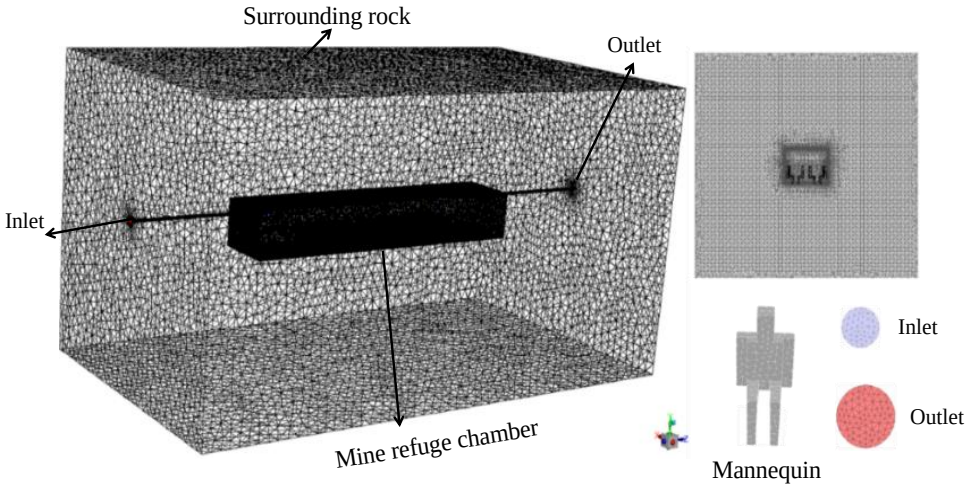

(b) Grid model

Fig. 3 Model of the 50-person MRC.

In the present study, ANSYS Fluent software was used for the numerical simulation. And a mesh independence study was conducted to identify an appropriate mesh density for the aimed calculations. Five meshes were investigated ranging from 2.25 million to 4.32 million cells. The mesh designation and number of cells are shown in Fig 4. compares the average AT value from the numerical calculation at 1 h and 3 h under five different grid models. It can be found that when the grid number is less than 3.49 million, the temperature value at the both moment changes significantly with the increase of the grid number, and when the grid number reaches 3.49 million, the temperature changes little with the increase of the grid number.

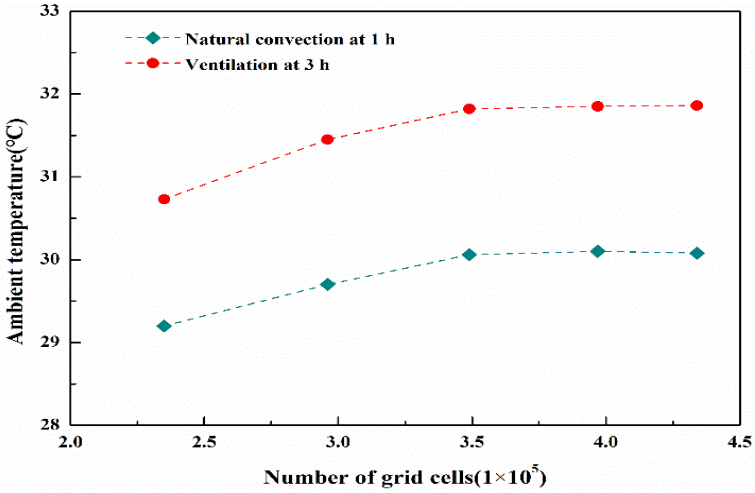

Fig. 4 Comparisons of numerical results under five different grid models.

2.3.2 Initial and boundary conditions

In the current work, a 50-person MRC with an ISRT of 35°C will be selected to analyze the thermal performance of the composite temperature control system. The boundary conditions of the body surfaces, air inlets and air outlets are defined as constant heat flow wall, velocity inlet and outflow, respectively. The surface in contact with the air calculation domain and the surrounding rock calculation domain is set as a coupling wall. Referred to the common SR of MRCs, the thermal conductivity, specific heat capacity and density of the SR are 2 W/(m·K), 920 J/(kg·K) and 2400 kg/m^3, respectively. The heat dissipation rate of occupants in the MRC is 120 W per capita when the refuge period. Separately, the heat flux on body surfaces was 0 W/m^2 during the time of SR pre-cooling and 60 W/m^2 during the refuge period. The VR for the MRC was the rated value of 0.3 m^3/min per capita, And the VT has been cooled to 20°C by the MCA cooling unit. Namely, at a speed of 6 m/s and a temperature of 20°C for all air inlets, the time of pre-cooling SR is 20, 30 and 40 days, respectively, after that, the time of refuge was 4 days.

To analyze the effect of several key impact factors such as ISRT, VR and VT on the performance of pre-cooling SR, the pre-cooling effect of the SR via continuous ventilation for 100 days under different parameters will be compared. The relevant parameters of these numerical cases are listed in Table 2.

Table 2 Parameters setting in numerical cases of SR pre-cooled via continuous ventilation for 100 days

Case 1	ISRT (°C)	VT (°C)	VR (m^3/h)
1	35	20	300
2	35	20	600
3	35	20	900
4	35	20	1200
5	35	20	1500
6	35	16	900
7	35	18	900
8	35	22	900
9	35	24	900

10	32	20	900
11	34	20	900
12	36	20	900
13	38	20	900
14	40	20	900

2.3.3 Turbulent model

Due to the strong performance in airflow, temperature and pressure for closed space [57], the Realizable *k-ε* turbulent model was adopt for the current numerical study. The enhanced wall treatment with pressure gradient effects and thermal effects, as well as the Boussinesq approximation were applied [58]. The governing equations, including continuity equation, momentum equation, and energy equation with Boussinesq, were given as follows [59].

$$\frac{\partial \rho}{\partial t} = -\frac{\partial (\rho u_i)}{\partial x_i} \tag{1}$$

$$\frac{\partial u_i}{\partial t} + \frac{\partial u_i u_j}{\partial x_j} = -\frac{1}{\rho}\frac{\partial P}{\partial x_i} + \frac{1}{\rho}\frac{\partial}{\partial x_j}[\mu(\frac{\partial u_i}{\partial x_j} + \frac{\partial u_j}{\partial x_i} - \rho\overline{u_i' u'}_j) - g_i\beta(T - T_0) \tag{2}$$

$$\frac{\partial T}{\partial t} + \frac{\partial (u_j T)}{\partial x_j} = \frac{1}{\rho}\frac{\partial}{\partial x_j}(\frac{\lambda}{C_p}\frac{\partial T}{\partial x_j} - \rho\overline{u_i' T'}) \tag{3}$$

where ρ is the air density, kg/m^3; t is the time, s; *xi* and x_j are the Cartesian coordinates in the *i* and *j* directions (*i*, *j* = 1, 2 and 3 corresponding to the *X*, *Y* and *Z* directions respectively); u_i and u_j are the mean fluid velocities in *X*, *Y* and *Z* directions, m/s; u'_i and $u'j$ are the corresponding fluctuant velocity components in the *i* and *j* directions, m/s; *P* is the mean air pressure, Pa; μ is the dynamic viscosity, Pa·s; g_i is the acceleration component of gravity in the i directions, m/s^2; β is the coefficient of thermal expansion, 1/K; *T* is the temperature, K; T_0 is the reference temperature, K; T' is the fluctuating temperature, K; λ is the air thermal conductivity, W/(m·K); C_p is the specific heat capacity, J/(kg·K).

The realizable *k-ε* model consists of the following two transport equations [60].

$$\frac{\partial}{\partial t}(\rho k) + \frac{\partial}{\partial x_j}(\rho k u_j) = \frac{\partial}{\partial x_j}[\frac{\partial k}{\partial x_j}(\mu + \frac{\mu_\tau}{\sigma_k})] + G_b + G_k + \rho\varepsilon \tag{4}$$

$$\frac{\partial}{\partial t}(\rho\varepsilon) + \frac{\partial}{\partial x_j}(\rho\varepsilon u_j) = \frac{\partial}{\partial x_j}[\frac{\partial \varepsilon}{\partial x_j}(\mu + \frac{\mu_\tau}{\sigma_\varepsilon})] + \rho C_1 S\varepsilon - \rho C_2 \frac{\varepsilon^2}{k + \sqrt{\nu\varepsilon}} + C_{1\varepsilon}\frac{\varepsilon}{k}C_{3\varepsilon}G_b \tag{5}$$

where *k* is the turbulent kinetic energy, J/kg; μ_τ is the turbulent viscosity, Pa·s; σ_k and σ_ε are the Prandt1 number; G_b is the generation of turbulence kinetic energy due to buoyancy, J/(s·m^3); G_k is the generation of turbulence kinetic energy due to the mean velocity gradients, J/(s·m^3); ε is the turbulent energy dissipation, J/(kg·s); *S* is the modulus of the mean rate-of-strain tensor; *v* is the kinematic viscosity, m^2/s; C_1, C_2, $C_{1\varepsilon}$, $C_{3\varepsilon}$ are model parameters.

In the present study, the pressure-velocity coupling solver and the pressure-implicit with splitting

of operators (PISO) are adopted. The pressure item is discretized by the body force weighted under natural convection and the standard under ventilation, respectively. The other items are discretized by the second-order upwind. Convergence criterion for energy item is 10^{-6}, while it is 10^{-3} for other items. For numerical cases under ventilation, the time step is initially 1 s, then gradually increased to 60 s after convergence. For numerical cases under natural convection, the time step is initially 0.1 s, then gradually increased to 1 s after convergence. It should be noted that the time step is related to the air velocity and minimum grid size, and the time step under ventilation and natural convection conditions is different because the air velocity of the two is different.

2.3.4 Model validation

The numerical model is validated by experimental results in Ref. [43]. The numerical cases of SR and air thermal parameters, thermal rate, ventilation parameters and other parameter settings are consistent with the experimental cases. Fig. 5 plots the comparative curves of the average AT and the deviation varies with time. It can be observed clearly that under three different ventilation states, the average AT obtained by numerical simulation agrees with the experiment data with a temperature difference less than 1°C. The deviation changes from 1.3% to 3.5%, indicating that the error caused by numerical calculation is small, and the numerical model is suitable for the following numerical analyses.

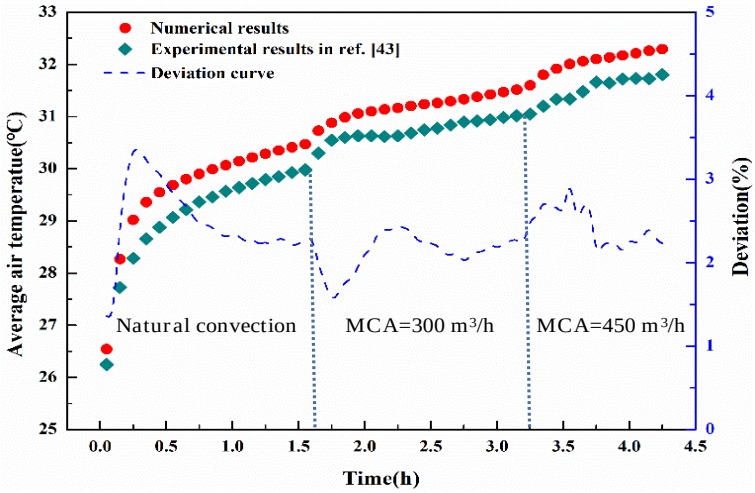

Fig. 5 Comparison of the average AT between experimental and numerical results.

3 Result

3.1 Thermal Performance of cooling MCA

Due to the temperature change of outside air entering the artificial room, the air inlet temperature has a slight oscillation during the process of experimental case 2 and 3, the average air inlet temperature is 36.13°C and 30.39°C, respectively.

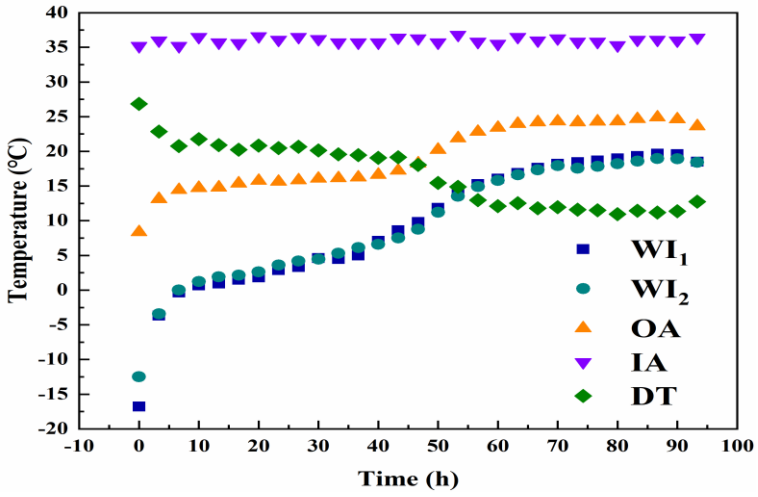

(a) Experimental case 1

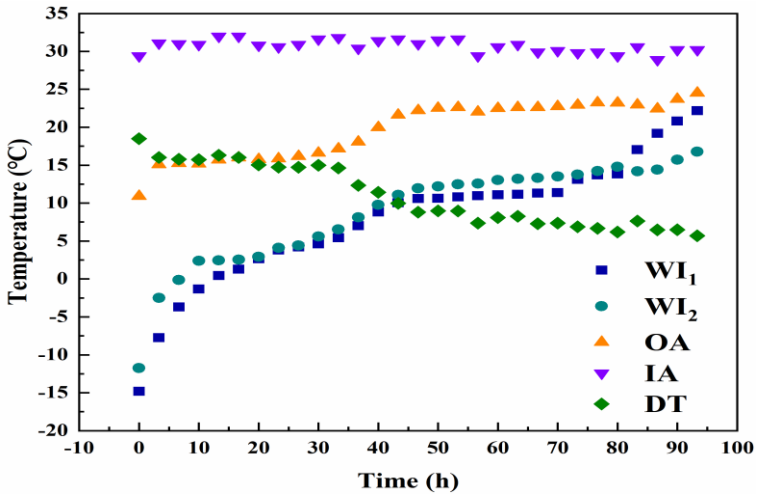

(b) Experimental case 2

Fig. 6 Temperature of the carrier and the MCA varies with time.

Fig. 6 plots the temperature variation of the MCA and the carrier with time within 96 h. In the figure, DT is the temperature difference between the inlet and outlet of the ice storage unit, IA is the inlet temperature, OA is the outlet temperature, and WI_1, WI_2 are the temperature changes in the tank. It can be observed that under a relatively stable air inlet temperature condition, the change in outlet air temperature will go through four stages. The first stage lasts about 6 ~ 8 h, in which the ice does not melt, the outlet air temperature increasing linearly with the time. The second stage lasts about 30 ~ 50 h, during this period there is a slight linear increase in the outlet air temperature over time, the heat of the MCA is absorbed during the melting of ice into water through the latent heat. The third stage lasts about 10 ~ 15 h, in which the outlet air temperature has a rapid linear upward trend, because the ice around the heat exchanger tube has all melted into water, the heat from the MCA is absorbed by water, but it can't be transferred quickly to the ice due to the small contact area between water and ice, resulting in quickly rise of the water temperature. The fourth stage lasts relatively long until all the ice is completely melted, during this period, the outlet air temperature rises slightly, because the ice melting rate has exceeded half, and the heat absorbed by the water can be quickly transferred to the ice through latent heat absorption due to sufficient thermal contact area.

Separately, from Fig. 6 (a) it can be observed that when the inlet air speed is 7 m/s, the temperature of the MRC can be cooled by the IS unit to below 20°C from about 36°C during the first 50 h, accompanying with a temperature difference of over 18°C. In the next 46 h, the outlet air temperature is basically maintained around 25°C. From Fig. 6 (b), it can be observed that when the inlet air speed is 11 m/s, the temperature of MRC can be cooled to below 20 °C from about 30°C during the first 48 h, and its value is less than 23°C in the next 48 h. The experimental results indicate that it is feasible to use the IS unit to cool the MCA, so as to storage cold source by the SR of the MRC during normal time or control temperature during the refuge period.

3.2 Thermal performance of the MCA-IS-SR system

3.2.1 Distribution of AT and SRT during pre-cooling

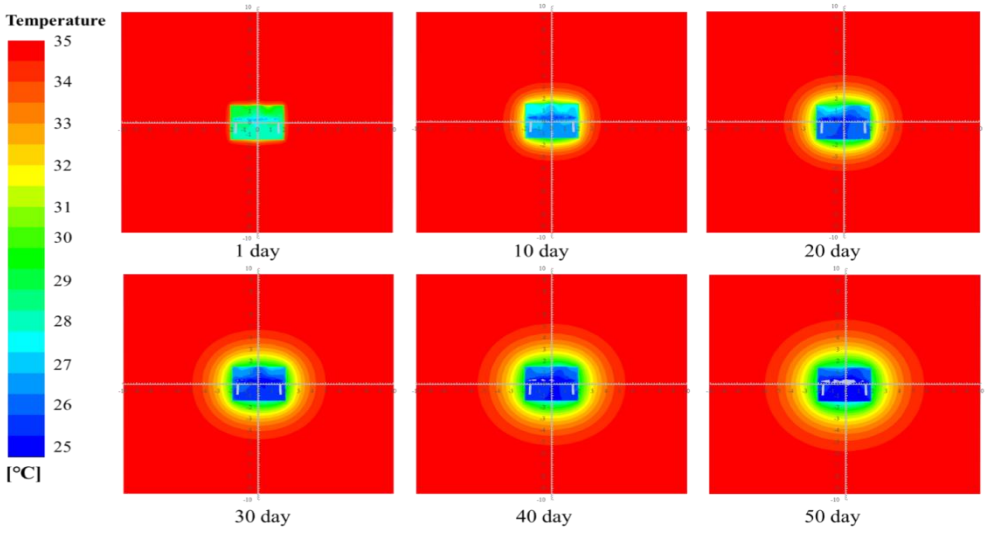

Fig. 7 Variation of the AT and the SRT at different times during pre-cooling

To observe the distribution characters of the AT and the SRT under the action of the cooled MCA with a VR of 900 m^3/h and a VT of 20°C, temperature clouds on the centre section surface of the MRC at different times, i.e., 1, 10, 20 ,30, 40 and 50 days, are compared. Fig. 7 displays the variation of the AT and the SRT under cooled MAC at different times. It can be observed that in the early stages, the AT is higher than the VT, because the air obtains heat in the dynamic heat transfer process between air and SR. With the increase of ventilation time, the AT gradually decreases. As far as the SR is concerned, when the ventilation lasts for a day, the SRT changes small, only a slight increase in temperature near the wall surface. While the ventilation lasts for 10 days, the temperature of the SR within 1 m decreases obviously. When the ventilation lasts for 20 days, the temperature of the SR beyond 1 m from the inner wall decreases in a circle from the inside to the outside, but the intensity gradually decreases, and the temperature variation of the SR beyond 2 m is hardly observed. As the ventilation time increases from 20 days to 50 days, although the SRT continues to decrease, the temperature variation of the SR beyond 3 m is not easy to be observed.

3.2.2 Variation of AT and SRT during pre-cooling

To know the variation of the SRT over time under the action of the cooled MCA with a VR of 900 m^3/h and a VT of 20°C. The SRT at 12 monitoring points varies with time within 50 days are compared. These points are located at 1.5 m above the floor on the centre section of the MRC, apart

from the inner wall surface 0, 0.5, 1, 1.5, 2, 2.5, 3, 4, 5, 6, 7 and 8 m, respectively.

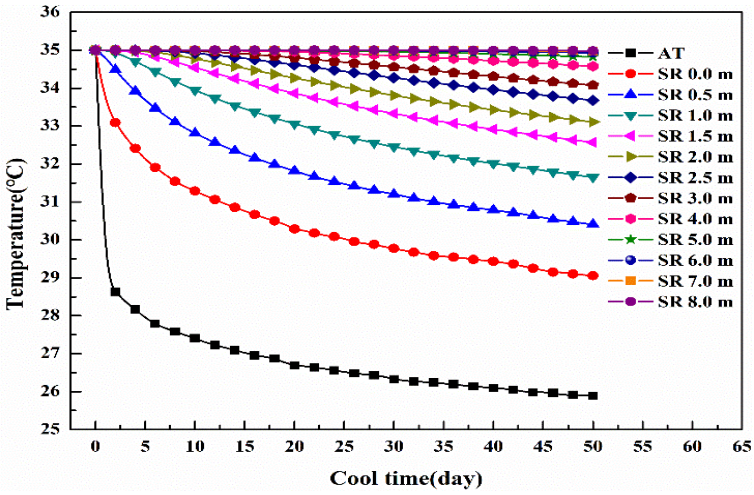

Fig. 8 Variation of the AT and the SRT with pre-cooling time within 50 days.

Fig. 8 plots the average AT and the SRT at different points change with time. It can be found that in the first 2 days, the average AT drops rapidly from 35°C to 28.8°C, then slowly decreases over time and keeps a relative stable temperature difference of 3 ~ 4°C with the SR surface, indicating that the heat transfer process between air and SR has entered a dynamic equilibrium state. The SRT decreases over time, occurring from the inner to outside. When the distance is in the range of 0 ~ 1.5 m, the SRT decreases curve with time, also its gradient decreases over time, because the heat obtained through the heat transfer between air and wall is absorbed by more volume of SR. When the distance exceeds 2 m, the SRT drops approximately linearly with time. With the increase of the distance, the intensity of the SRT drop is weakening. After the ventilation lasts for 5, 10, 20 and 40 days, respectively, the SRT at 1.5, 2.5, 4 and 5 m begins decrease sequentially. However, after 50 days of ventilation, it is still difficult to observe the temperature of SR at the 6 m position drop.

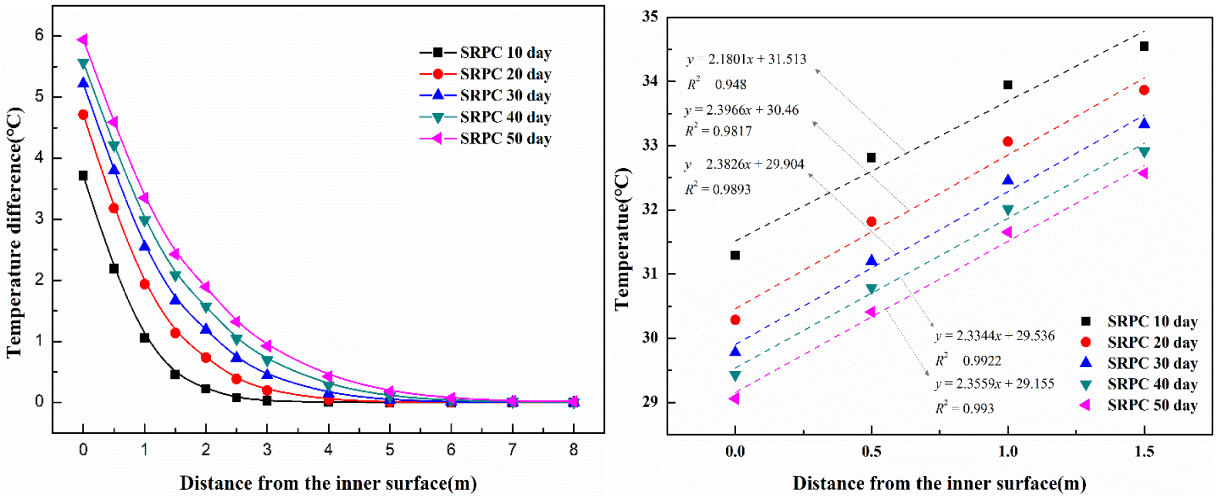

(a) Temperature difference of SR from 0 ~ 8 m at different times (b) SRT from 0 to 1.5 m at different times

Fig. 9 Variation of the SRT with the distance from the inner surface at different times.

Fig. 9 (a) plots the temperature difference of SR from 0 ~ 8 m at different times. It can be observed that at a same moment, the temperature difference of SR decreases exponentially with distance. Among them, from 0 to 1.5 m, the temperature difference decreases the fastest with distance,

which is approximately linear, while the distance is over 3 m, the temperature difference becomes little, indicating that during the pre-cooling time, the cold capacity is mainly stored in the SR within 3 m. At the same point, the longer the ventilation time, the greater the temperature difference of SR. Fig. 9 (b) plots the temperature of SR from 0 to 1.5 m points at five different times. It can be found that during the SR pre-cooling time, the SRT has an obvious linear relationship with the distance within 1.5 m. With the increase of time, the linear relationship becomes much more significant.

3.2.3 Performance of the MCA-IS-SR system during taking shelter

To know the temperature control characteristics of the MCA-IS-SR scheme, the MRC with an ISRT of 35℃ has been pre-cooled by the cooled MCA with a VT of 20℃ and a VR of 900 m^3/h for 30 days. After that, a HR of 6 kW is released from the 50 human body surfaces and the ventilation lasts for 4 days without changing the parameters of ventilation.

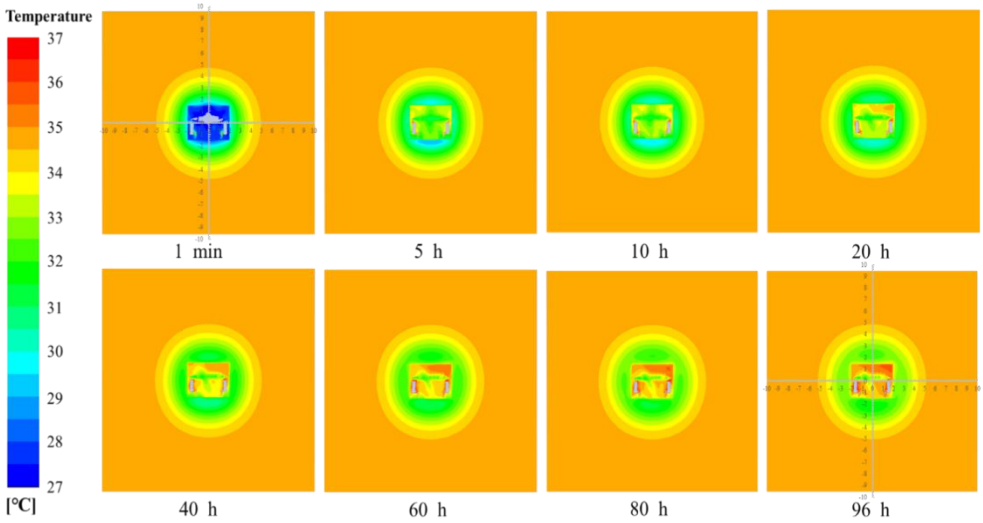

Fig. 10 Distribution of AT and SRT under cooled MAC at different times.

Fig. 10 displays the variation of the AT and the SRT under the cooled MAC at different times during taking shelter. It can be found that at the initial moment, the temperature distribution of the SR is non-uniform and the AT is lower than 28°C. Specifically, the SRT gradually decreases from the inside to the outside in the range of 0 ~ 3 m, and the temperature of the SR beyond 3 m remains constant. For the SR within 1 m apart from the inner wall surface, the bottom has the lowest temperature, followed by the top, while the both-sides has a relatively high temperature. The AT is gradually rising with the increase of time, yet not beyond 35°C overall at the first 40 h. At 60 h, the AT in the upper space reaches 36°C, while in the lower part its value is still below 35°C. At 96 h, the AT in the lower space of human activity is close to 35°C.

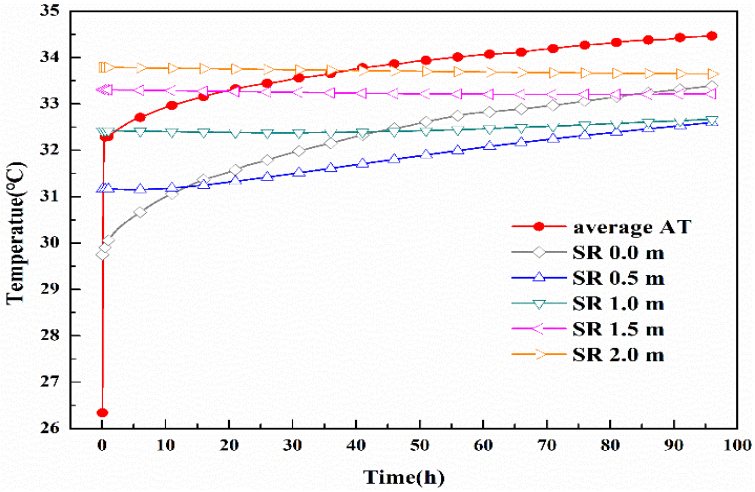

Fig. 11 Temperature varies with time during 96 h of taking shelter.

Fig. 11 plots the average AT and the SRT at different distance varying with time within 96 h. It can be found that although the AT increases gradually with time, it does not exceed 35℃ at 96 h, indicating that the temperature control requirement of the MRC with an ISRT of 35℃ can be met through the MCA-IS-SR scheme. The temperature change trend of the SR on the inner surface is similar to that of the AT. As the distance increases, the temperature change of the SR gradually weakens. The SRT at 1 m increases by about 0.3°C within 96 h. The SRT at 1.5 m still keeps a slight downward trend in the first 80 h, decreasing by about 0.2°C, after that, about 0.1°C is increased in the next 16 h. The SRT at 2 m maintains a slight downward trend within 96 h, dropping by about 0.3°C. It can be concluded that during the 96 h of taking shelter, only the cold energy stored by SR in the range of 1.5 m plays a positive role in the temperature control of the MRC.

3.2.4 Prediction of AT in the MRC during taking shelter

To predict the AT of MRCs with pre-cooled SR during the time of taking shelter, keeping the same ventilation and HR, i.e., the VT is 900 m^3/h, the VT is 20°C and the HR is 6 kW, the AT curves of the MRC with pre-cooled SR and the MRC with equivalent ISRT will be compared. For the MRC with an ISRT of 35°C, after being pre-cooled by the cooled MCA for 20, 30 and 40 days, the equivalent ISRTs are 32.25, 31.7 and 31.27°C, respectively.

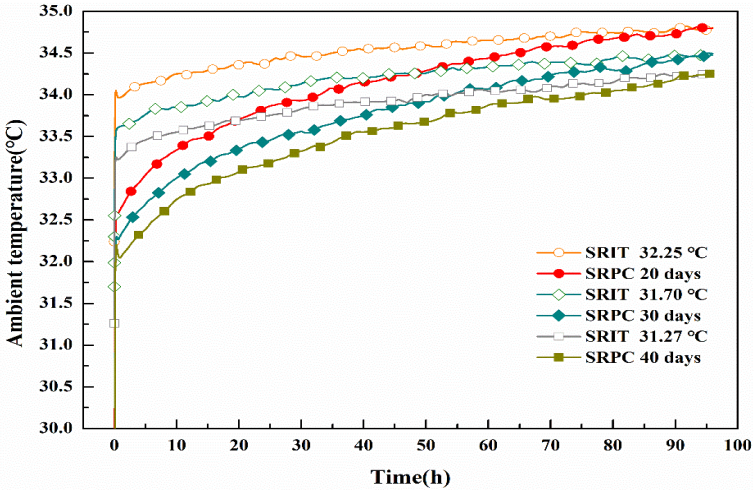

Fig. 12 Comparison of AT varies with time under the three different conditions.

Fig. 12 compares the variation curves of the AT within 96 h for the MRC with the pre-cooled SR and the MRC with the equivalent ISRT under the same ventilation conditions. It can be found that for the three different cases, the AT of the MRC with pre-cooled SR is essentially equal to that of the MRC with the equivalent ISRT at the moment of 96 h. Previously, the MRC with pre-cooled SR has lower AT than the MRC with equivalent ISRT, because the former has a lower temperature near the inner wall surface, which allows more heat from the breathing environment to be absorbed. Overall, for the MRC with pre-cooled SR, the average temperature of the SR within 1.5 m can be regarded as an equivalent ISRT, then the AT of the MRC at the moment of 96 h can be predicted.

3.3 Sensitive analyse during pre-cooling

Since the average temperature of the pre-cooled SR within 1.5 m plays an important role in the temperature control performance of the MRC when taking shelter, the average temperature of SR within 1.5 m varies over time are compared during the SR pre-cooling time.

3.3.1 Effect of the VR

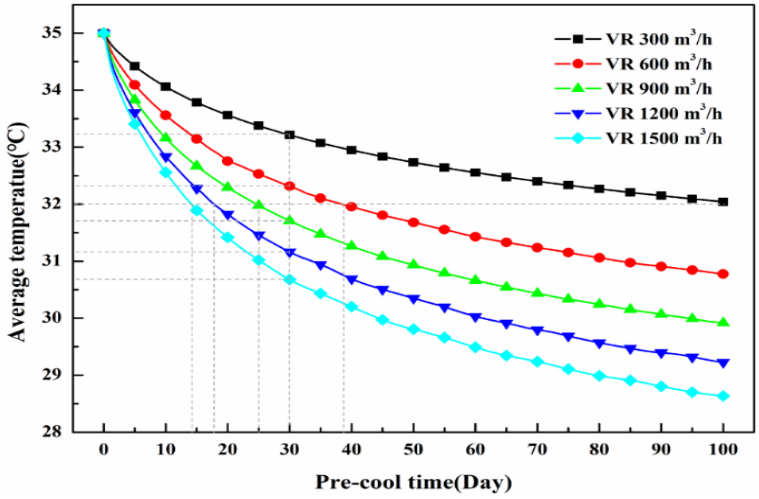

Fig. 13 Average temperature of SR within 1.5 m under different VR.

Fig. 13 plots the average temperature of SR within 1.5 m varies with time under different VR. It can be found that the average temperature drops exponentially over time. With the increase of VR, the gradient of the SRT increases, but the intensity of the gradient increase becomes weaker at the same moment, for example, at 30 days of continuous ventilation by the MCA, the average temperature of the SR decreased by 1.79, 2.69, 3.30, 3.83 and 4.31°C at a VR of 300, 600, 900, 1200 and 1500 m^3/h, respectively. In addition, taking the average SR temperature of 32°C as the cold energy storage target, when the VR is 600, 900, 1200 and 1500 m^3/h, the continuous ventilation time is 38.5, 25, 18 and 14 days, respectively.

3.3.2 Effect of the VT

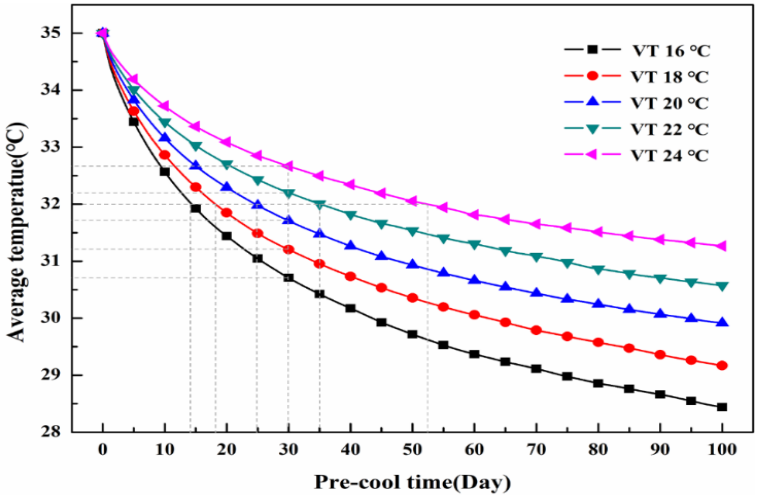

Fig. 14 Average temperature of SR within 1.5 m under different VT.

Fig. 14 plots the average temperature of SR within 1.5 m varies with the cooling time under different VT. It can also be seen that the average temperature of the surrounding rock thickness within 1.5 meters is exponentially related to time and decreases with increasing time. With the increase of VT, the gradient of the SRT decreases, but the intensity of the gradient increase keeps the same at the same moment, for example, at 30 days, the average drop temperature of the SR increases by 0.49 °C for every 2°C increase in VT. Taking the average SR temperature of 32°C as the goal of cold storage, when the VT is 16, 18, 20, 22 and 24°C, the continuous ventilation time is 14, 18, 25, 35 and 52.5 days, respectively.

3.3.3 Effect of the ISRT

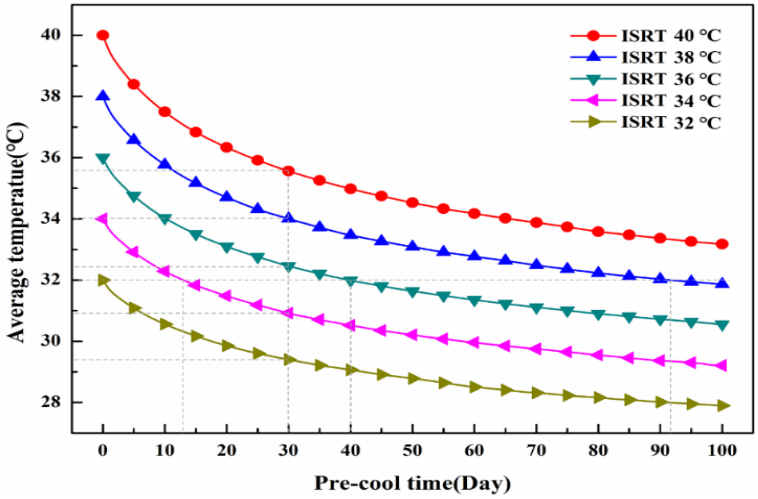

Fig. 15 Average temperature of SR within 1.5 m under different ISRT.

Fig. 15 plots the average temperature of SR within 1.5 m varies with the pre-cooling time under different ISRT. Similarly, it can be found that the average temperature of the SR within 1.5 m drops exponentially with time. However, the ISRT has little effect on the gradient of the SRT drop. At 30 days, the average drop temperature of the SR increases by 1.6°C for every 2°C increase in ISRT. Taking the average SR temperature of 32°C as the goal of cold storage, when the ISRT is 34, 36 and 38°C, the continuous ventilation time is 13, 40 and 92 days, respectively.

3.4 Thermal recovery of the pre-cooled SR

To analyze the thermal recovery performance of the pre-cooled SR, the SR with an ISRT of 35°C has been pre-cooled by continuous ventilation with a VT of 20°C and a VR of 900 m^3/h for 30 days, then exposed to a natural convection environment for 30 days.

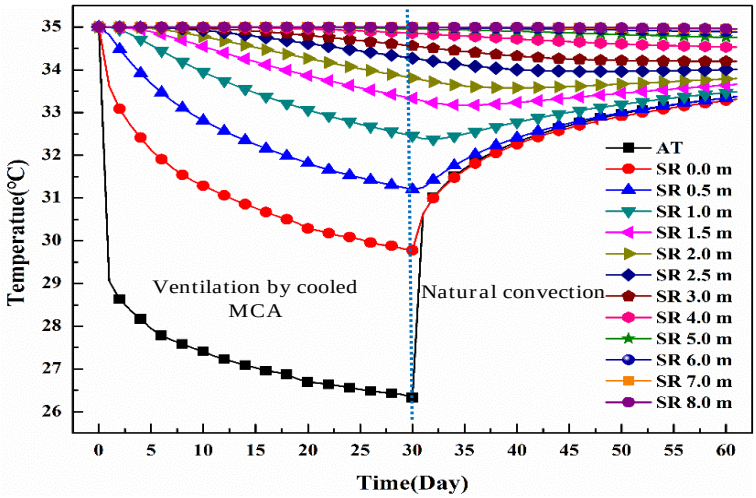

Fig. 16 Temperature variation of the pre-cooled SR with time under natural convection.

Fig. 16 plots the temperature variation curves of SR pre-cooled 30 days varying with time under natural convection. It can be found that under natural convection, the temperature on the surface of the SR has an obvious recovery, and the AT has a similar trend with the temperature on the surface, following with temperature difference less than 0.2°C. As the depth increases, the less the rock temperature recovers. After 30 days of ventilation by cooled MCA, the temperature of rocks at 0, 0.5, 1 and 1.5 m decreased by 5.22, 3.78, 2.55 and 1.67°C, respectively, and the average temperature of SR within 1.5 m decreased by 3.31°C. In contrast, after 30 days of natural convection, the temperature of pre-cooled SR at 0, 0.5 m, 1 and 1.5 m recovered by 3.50, 2.14, 1.01 and 0.31°C, respectively, and the average temperature of SR within 1.5 m recovered by 1.74°C. The ratio of the temperature at which the surrounding rock recovers to the temperature at which the surrounding rock pre-cooling down is called the recovery rate, with a recovery ratio of about 53%, indicating that during the cold preservation period of the pre-cooled SR, when the ratio of ventilation time to non-ventilation time is 53:100, the average temperature of the pre-cooled SR within a depth of 1.5 m can be basically unchanged.

4 Discussion

4.1 Economics of the MCA-IS-SR system

4.1.1 Comparison of a device cost

As available alternative cooling schemes for MRCs, two existing ISACs has been reported, including a forced-circulation ISAC with an ice storage capacity of 5.34 m^3 [34] and a multifunctional ISAC with an ice storage volume of 1.8 m^3 [37]. However, both devices require explosion-proof fans to drive the indoor hot air to flow through the heat exchange channel of the device, then the cooled air return to the indoor environment to achieve the cooling function. In addition, both devices need to be equipped with explosion-proof batteries with sufficient storage capacity to meet the power

consumption needs of explosion-proof fans in 96 h. Compared with the existing two devices, when using the MCA-IS-SR scheme, the cost of MCA-ISAC will be greatly reduced, because it does not need to be equipped with explosion-proof fans and explosion-proof batteries. Meanwhile, the operating and maintenance costs of the equipment will be significantly reduced during the five-year service period, as there is no need to charge the battery and maintain the fan and battery. According to a survey result of market and user, Table 3 compares the critical component cost, operating cost and installation cost between the existing ISAC and the MCA-ISAC, in the case of an ice storage capacity of 1 m^3. It can be known that compared with the price of ¥ 80,000 for the existing ISAC, the price of the MCA-ISAC has decreased by 50%. At the same time, its annual operating costs will be cut in half, about ¥ 3000. Compared with the existing ISAC, MCA-ISAC saves the installation cost of explosion-proof fan and explosion-proof battery, but increases the installation cost of MCA duct, so the actual installation cost is basically the same.

Table 3 Comparison of equipment cost and operating cost between the existing ISAC and the MCA-ISAC

Item	Existing ISAC	MCA-ISAC
Critical component costs	Ice storage tank, ¥ 3000	Ice storage tank, ¥ 3000
	Heat exchange component, ¥ 2000	Heat exchange component, ¥ 7000
	Refrigeration compressor, ¥ 30,000	Refrigeration compressor, 30,000
	Explosion-proof fan, ¥ 10,000	/
	Explosion-proof battery, ¥ 35,000	/
Operating costs	Ice storage process, ¥ 2000 per year	Ice storage process, ¥ 2000 per year
	Battery charging process, ¥ 2000 per year	MCA ventilating process, ¥ 500 per year
	Maintenance, ¥ 2000 per year	Maintenance, ¥ 500 per year
Installation costs	Ice storage unit install, ¥ 2000	Ice storage unit install, ¥ 2000
	Explosion-proof fan install, ¥ 500	MCA duct install, ¥ 1000
	Explosion-proof battery install, ¥ 500	

4.1.2 Comparison of the system cost in MRC

Taking the above 50-person MRC with an ISRT of 35℃ as the object, economics of three temperature control schemes including the existing IS, the MCA-IS and the MCA-IS-SR, will be compared. The total heat dissipation from the human bodies is about 2.07×10^6 kJ within 96 h [24]. Assuming that the AT keeps a constant of 35℃ during the taking shelter time, meaning that there is no heat exchange between the air and the SR.

When the MCA-IS scheme is adopted, the average AT in the MRC after 1 h of ventilation can be calculated as follow [43].

$$T_a(\tau) = [(1.35T_v - 1.3T_{isr} + 4.63Q) \times 10^{-2} + 0.7e^{-0.002G} - 0.16]\sqrt{\tau} + 0.27T_v + 0.7T_{isr} - 0.003G + 0.8Q + 4 \quad (6)$$

Where, T_a is the AT in the MRC, ℃; τ is the ventilating time, h; T_v is the VT, ℃; T_{isr} is the ISRT, ℃; Q is the HR generated by occupants, kJ; G is the VR, m^3/h.

Assuming that the AT of the MRC at 96 h is 35℃, thus, when the VR is 900 m^3/h and the HR is 6 kW, according to eq. (6), the relation between the VT and the ISRT can be written as

$$T_v = 66.78 - 1.45T_{isr} \quad (7)$$

Since the MCA entering the MRC needs to be transported through a long-distance pipeline, the

temperature of the MCA is close to the ISRT. According to Newton cooling law, the required cold capacity for the MRC temperature controlling within 96 h can be calculated as

$$Q_m = \rho C_p G(T_{mca} - T_v)\tau = 96\rho C_p G(T_{isr} - T_v) = (2.73T_{isr} - 74.43) \times 10^5 \quad (8)$$

Where, Q_m is the cold capacity for a MRC, kJ; T_{mca} is the temperature of MCA entering the MRC, ℃.

Furtherly, the number of IS units for the MRC is calculated as

$$n = Q_m/q \quad (9)$$

Where, n is the number of IS units for MRC; q is the cold capacity of an IS unit, kJ.

It can be calculated from eq. (8) and (9) that, for the 50-person MRC with an ISRT of 35℃, also about 5 IS devices are required when the MCA-IS scheme is adopted. The cost of the MCA-IS system is ¥ 265,000, consisting of ¥ 250,000 in equipment cost and ¥ 15,000 in operating cost during 5-year service period, which is about 38% less in the cost than the existing IS system.

When the MCA-IS-SR scheme is adopted, assuming that the SRT has been pre-cooled to the equivalent ISRT, in the case of a VR of 900 m^3/h, the relationship between the VT and the equivalent ISRT is expressed as follow

$$T_v = 66.78 - 1.45\,T_{eisr} \quad (10)$$

Where, T_{eisr} is the equivalent ISRT, ℃.

Assuming that the T_{mca} is equal to the ISRT, for the MRC with an ISRT of 35℃, according to Newton cooling law, the required cold capacity for the MRC temperature controlling within 96 h can be calculated as follow

$$Q_m = \rho C_p G(T_{mca} - T_v)\tau = (1.616\,T_{eisr} - 35.421) \times 10^5 \quad (11)$$

According to Eqs. (9) and (11), when the equivalent SRT was pre-cooled to 32.2℃ and 29.6℃ after 22 days and 110 days, respectively, the number of devices was reduced to 4 and 3 for the MRC with an ISRT of 35℃ to meet the temperature control requirement within 96 h.

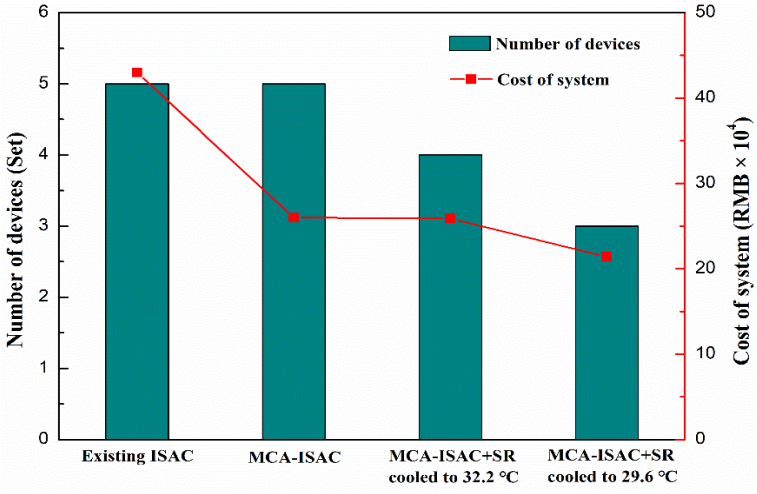

Fig. 17 Economic comparison of different cooling schemes

Fig. 17 compares the cost of the temperature control system over a five-year period of service under different temperature control schemes. It can be found that when the SR is not used as a cold storage medium, although the number of devices required for the existing ISAC scheme and the MCA-ISAC scheme is the same, the cost of the latter is reduced by ¥ 170,000, a reduction of about 40%. When the MCA-ISAC-SR is adopted, the number of devices will be reduced to 4 after the SR

is pre-cooled to an equivalent temperature of 32.2℃ from the ISRT of 35℃. Whereas, compared to the MCA-ISAC scheme, its cost only decreases by about 0.4%, because the cost of cold storage via the SR and maintenance over a five-year service period is close to the cost of one device. Furthermore, by pre-cooling the SR to an equivalent temperature of 29.6℃, the number of devices will decrease to 3, resulting in a cost reduction of approximately ¥ 46,000 with a decrease of about 17.7%, compared to the MCA-ISAC scheme. It can be deduced that for MRCs with an ISRT of 32℃ or more, the economy of the MCA-IS-SR scheme will reflect after the SR is cooled to equivalent 32℃ or below.

4.2 Cooling schemes for MRCs with different ISRT

Thanks to the cold radiation of the low-temperature SR, cooling measures are not necessary for MRCs with an ISRT of 20°C or less [61]. When the VR is 0.1 m^3/min per capita for a MRC, the CO_2 concentration, O_2 supply and the RH can be kept at the safe level [24,28,29], even more, the AT cannot over 35°C at 96 h if the ISRT is not more than 25°C [25]. When the VR is 0.3 m^3/min per capita, the MCA can keep the AT of the MRC below 35°C under the condition that the ISRT is below 27°C [27]. While the VR reaches 0.5 m^3/min per capita, the MCA can meet the temperature control requirement of the MRC with an ISRT of 30°C, according to eq. (11). Practically, for most MRCs, the VR will not more than 0.3 m^3/min per capita, so the temperature control scheme of MCA-IS was recommend for MRCs with ISRT above 27°C [43]. However, considering the cost, the improved temperature control scheme of MCA-IS-SR is more worthy of promotion for MRCs with an ISRT of above 32°C. The temperature control scheme for MRCs with different ISRT can refer to Table 4.

Table 4 Economical temperature control scheme for a MRC with different ISRTs.

ISRT of the MRC	Recommended scheme	Air supply volume per capita (m^3/min)	Number of people served by each ISD
20°C or less	Not required	0.1	/
20 ~ 25°C	MCA	0.1	/
25 ~ 27°C	MCA	0.1 ~ 0.3	/
27 ~ 30°C	MCA	0.3 ~ 0.5	/
	& MCA-IS	0.3	20 ~ 25
30 ~ 32°C	MCA-IS	0.3	15 ~ 20
32°C or more	MCA-IS-SR	0.3	10 ~ 15

5 Conclusion

An improved composite temperature control scheme combining MCA, IS and SR was proposed for MRCs with high ISRT. The feasibility of using IS unit to cool the MCA was tested. On this basis, thermal performance of the improved scheme applied to MRC with high ISRT was studied by numerical simulation. In addition, the economy of the improved scheme was discussed. The following specific conclusions can be drawn:

(1) It is feasible to use the ice storage unit to cool the mine compressed air, the mine compressed air temperature will reduce by 15 ~ 18°C at the first 30 h and by 6 ~ 8°C within 40 ~ 96 h when the air volume is 300 m^3/h.

(2) With the increase of distance, the intensity of surrounding rock temperature drop is

weakening, the surrounding rock temperature within 1.5 m decreases approximately linearly with the distance, which can be regarded as an equivalent initial surrounding rock temperature to predict the ambient temperature of the mine refuge chamber at 96 h.

(3) For a mine refuge chamber with an initial surrounding rock temperature of 35°C, when the ventilation temperature is 0.3 m^3/min per capita and the ventilation temperature is 20°C, the average ambient temperature can maintain below 34.5°C within 96 h, after the surrounding rock has been pre-cooled by continuous ventilation for 30 days.

(4) During pre-cooling, the surrounding rock temperature drops exponentially over time, the temperature gradient decreases with the ventilation rate and the ventilation temperature, but has little to do with the initial surrounding rock temperature. The temperature of the pre-cooled surrounding rock changes little when the ratio of ventilation time to non-ventilation time is 53:100.

(5) After 30 days of ventilation by cooled MCA, the average temperature of SR within 1.5 m decreased by 3.31℃. After 30 days of natural convection, the average temperature of SR within 1.5 m recovered by 1.74℃, with a recovery ratio of about 53%.

(6) For mine refuge chambers with an initial surrounding rock temperature of 32℃ or more, the economy of the mine compressed air-ice storage-surrounding rock scheme will reflect after the surrounding rock is cooled to equivalent 32℃ or below.

Declaration of competing interest

The authors declare that they have no known competing financial interests or personal relationships that could have appeared to influence the work reported in this paper.

Acknowledgments

The authors would like to thank the financial support from the National Natural Science Foundation of China (52168013), the Natural Science Foundation of Guizhou Province (ZK[2022]151) and the State Key Laboratory of Gas Disaster Detecting, Preventing and Emergency Controlling Open-fund Project (2021SKLKF10).

References

[1] K. Guerra, R. Gutiérrez-Alvarez, O.J. Guerra, P. Haro, Opportunities for low-carbon generation and storage technologies to decarbonise the future power system, Appl. Energy 336 (2023) 120828, https://doi.org/10.1016/j.apenergy.2023.120828.

[2] X. Zheng, Y. Zhou, A three-dimensional unsteady numerical model on a novel aerogel-based pv/t-pcm system with dynamic heat-transfer mechanism and solar energy harvesting analysis, Appl. Energy 338 (2023) 120899, https://doi.org/10.1016/j.apenergy.2023.120899.

[3] M.T. Ameen, Z. Ma, A. Smallbone, R. Norman, A.P. Roskilly, Experimental study and analysis of a novel layered packed-bed for thermal energy storage applications: a proof of concept, Energy Conv. Manag. 277 (2023) 116648, https://doi.org/10.1016/j.enconman.2022.116648.

[4] C. Semeraro, A.G. Olabi, H. Aljaghoub, A.H. Alami, M. Al Radi, M. Dassisti, M.A. Abdelkareem, Digital twin

application in energy storage: trends and challenges, J. Energy Storage 58 (2023) 106347, https://doi.org/10.1016/j.est.2022.106347.

[5] O. Mahian, M. Javidmehr, A. Kasaeian, S. Mohasseb, M. Panahi, Optimal sizing and performance assessment of a hybrid combined heat and power system with energy storage for residential buildings, Energy Conv. Manag. 211 (2020) 112751, https://doi.org/10.1016/j.enconman.2020.112751.

[6] M. Deymi-Dashtebayaz, I.V. Baranov, A. Nikitin, V. Davoodi, A. Sulin, M. Norani, V. Nikitina, An investigation of a hybrid wind-solar integrated energy system with heat and power energy storage system in a near-zero energy building-a dynamic study, Energy Conv. Manag. 269 (2022) 116085, https://doi.org/10.1016/j.enconman.2022.116085.

[7] L. Hu, Y. Liu, D. Wang, X. Luo, H. Liu, Feasibility analysis and feature comparison of cold thermal energy storage for off-grid pv air-conditioned buildings in the tropics, Energy Conv. Manag. 254 (2022) 115176, https://doi.org/10.1016/j.enconman.2021.115176.

[8] M. Barthwal, A. Dhar, S. Powar, The techno-economic and environmental analysis of genetic algorithm (ga) optimized cold thermal energy storage (ctes) for air-conditioning applications, Appl. Energy 283 (2021) 116253, https://doi.org/10.1016/j.apenergy.2020.116253.

[9] J. Cho, J. Woo, Development and experimental study of an independent row-based cooling system for improving thermal performance of a data center, Appl. Therm. Eng. 169 (2020) 114857, https://doi.org/10.1016/j.applthermaleng.2019.114857.

[10] B.B. Kanbur, C. Wu, S. Fan, F. Duan, System-level experimental investigations of the direct immersion cooling data center units with thermodynamic and thermoeconomic assessments, Energy 217 (2021) 119373, https://doi.org/10.1016/j.energy.2020.119373.

[11] C. Zeng, Y. Yuan, F. Haghighat, K. Panchabikesan, X. Cao, L. Yang, Z. Leng, Thermo-economic analysis of geothermal heat pump system integrated with multi-modular water-phase change material tanks for underground space cooling applications, J. Energy Storage 45 (2022) 103726, https://doi.org/10.1016/j.est.2021.103726.

[12] X. Gao, Y. Xiao, P. Gao, Thermal potential improvement of an earth-air heat exchanger (eahe) by employing backfilling for deep underground emergency ventilation, Energy 250 (2022) 123783, https://doi.org/10.1016/j.energy.2022.123783.

[13] K.A. Margolis, C.Y.K. Westerman, K.M. Kowalski-Trakofler, Underground mine refuge chamber expectations training: program development and evaluation, Saf. Sci. 49 (3) (2011) 522-530, https://doi.org/10.1016/j.ssci.2010.12.008.

[14] C. Mejías, D. Jiménez, A. Muñoz, L. Reyes-Bozo, Clinical response of 20 people in a mining refuge: study and analysis of functional parameters, Saf. Sci. 63 (2014) 204-210, https://doi.org/10.1016/j.ssci.2013.11.011.

[15] Z. Zhang, Y. Yuan, K. Wang, X. Gao, X. Cao, Experimental investigation on influencing factors of air curtain systems barrier efficiency for mine refuge chamber, Process Saf. Environ. Protect. 102 (2016) 534-546, https://doi.org/10.1016/j.psep.2016.05.008.

[16] E. Paul Meisburger, D. Iryanto, D. Quinn, A. Widyastutie, A. Mone, Design and construction of high capacity fixed refuge chambers at pt freeport indonesia's underground operations, in: X. Chang (Ed.), Springer Singapore, Singapore, 2019, pp. 850-859. https://doi.org/10.1007/978-981-13-1420-9_73

[17] K.E. Karadeniz, S. Nowak, D. Guner, T. Sherizadeh, Evaluation on underground refuge alternatives and explosion survivability: a review, Mining, Metallurgy & Exploration 39 (6) (2022) 2311-2331, https://doi.org/10.1007/s42461-022-00682-1.

[18] Z. Shao, Y.C. Yang, M. Kumral, Optimal refuge chamber position in underground mines based on tree network, Int. J. Inj. Control Saf. Promot. 30 (2) (2023) 294-309, https://doi.org/10.1080/17457300.2022.2164311.

[19] Y. Li, Y. Yuan, C. Li, X. Han, X. Zhang, Human responses to high air temperature, relative humidity and carbon dioxide concentration in underground refuge chamber, Build. Environ. 131 (2018) 53-62, https://doi.org/10.1016/j.buildenv.2017.12.038.

[20] D.Y.M.K. L. Yan, Validation of temperature and humidity thermal model of 23-person tent-type refuge alternative. Society for mining, Metallurgy, and Exploration (340) (2016) 225-231, http://dx.chinadoi.cn/http://dx.doi.org/10.19150/me.6759.

[21] B. Yang, H. Yao, P. Yang, Y. Guo, F. Wang, C. Yang, A. Li, L. Che, Effects of thermal and acoustic environments on workers' psychological and physiological stress in deep underground spaces, Build. Environ. 212 (2022) 108830, https://doi.org/10.1016/j.buildenv.2022.108830.

[22] R. Qiao, X. Li, S. Gao, X. Ma, Improvement of thermal comfort for underground space: data enhancement using variational autoencoder, Build. Environ. 207 (2022) 108457, https://doi.org/10.1016/j.buildenv.2021.108457.

[23] D.S.Y.E. T. Bernard, estimation of metabolic heat input for refuge alternative thermal testing and simulation, Min. Eng. (70) (2018) 50-54, https://doi.org/10.19150/me.8429.

[24] Z. Zhang, T. Jin, H. Wu, R. Day, X. Gao, K. Wang, R. Mao, Experimental investigation on environmental control of a 50-person mine refuge chamber, Build. Environ. 210 (2022) 108667, https://doi.org/10.1016/j.buildenv.2021.108667.

[25] Z. Zhang, H. Wu, K. Wang, R. Day, Y. Yuan, Thermal performance of a mine refuge chamber with human body heat sources under ventilation, Appl. Therm. Eng. 162 (2019) 114243, https://doi.org/10.1016/j.applthermaleng.2019.114243.

[26] A.E. Halim, J.F. Brune, Do refuge chambers represent a good strategy to manage emergencies in underground coal mines? Mining, Metallurgy & Exploration 36 (6) (2019) 1191-1199, https://doi.org/10.1007/s42461-019-0100-8.

[27] X. Gao, Z. Zhang, Y. Xiao, Modelling and thermo-hygrometric performance study of an underground chamber with a long vertical earth-air heat exchanger system, Appl. Therm. Eng. 180 (2020) 115773, https://doi.org/10.1016/j.applthermaleng.2020.115773.

[28] Z. Zhang, H. Wu, K. Wang, R. Day, Y. Yuan, Air quality control in mine refuge chamber with ventilation through pressure air pipeline, Process Saf. Environ. Protect. 135 (2020) 46-58, https://doi.org/10.1016/j.psep.2019.12.014.

[29] H. Shao, S. Jiang, W. Tao, Z. Wu, W. Zhang, K. Wang, Theoretical and numerical simulation of critical gas supply of refuge chamber, Int. J. Min. Sci. Technol. 26 (3) (2016) 389-393, https://doi.org/10.1016/j.ijmst.2016.02.004.

[30] D.S. Yantek, L. Yan, N.W. Damiano, M.A. Reyes, J.R. Srednicki, A test method for evaluating the thermal environment of underground coal mine refuge alternatives, Int. J. Min. Sci. Technol. 29 (3) (2019) 343-355, https://doi.org/10.1016/j.ijmst.2019.01.004.

[31] D.S. Yantek, L. Yan, P.T. Bissert, M.D. Klein, Effects of mine strata thermal behavior and mine initial temperatures on mobile refuge alternative temperature, Min. Eng. 4 (69) (2017) 41-48, https://doi.org/10.19150/me.7393.

[32] L. Yan, D.S. Yantek, M.A. Reyes, Underground mine air and strata temperature change due to the use of refuge alternatives, Mining, Metallurgy & Exploration 37 (2) (2020) 773-781, https://doi.org/10.1007/s42461-019-00153-0.

[33] B.C.C.V. Friedenstein, Simulating operational improvements on mine compressed air systems, The South African Journal of Industrial Engineering 3 (29) (2018) 69-81, https://doi.org/10.7166/29-3-2049.

[34] S. Wang, L. Jin, Z. Han, Y. Li, S. Ou, N. Gao, Z. Huang, Discharging performance of a forced-circulation ice thermal storage system for a permanent refuge chamber in an underground mine, Appl. Therm. Eng. 110 (2017) 703-709, https://doi.org/10.1016/j.applthermaleng.2016.08.192.

[35] Y. Jia, Y. Liu, S. Sun, H. Li, L. Jiao, Refrigerating characteristics of ice storage capsule for temperature control of coal mine refuge chamber, Appl. Therm. Eng. 75 (2015) 756-762, https://doi.org/10.1016/j.applthermaleng.2014.10.036.

[36] X. Xu, S. You, X. Zheng, H. Zhang, S. Liu, Cooling performance of encapsulated ice plates used for the underground refuge chamber, Appl. Therm. Eng. 112 (2017) 259-272, https://doi.org/10.1016/j.applthermaleng.2016.10.072.

[37] Y. Du, W. Gai, L. Jin, W. Sheng, Thermal comfort model analysis and optimization performance evaluation of a multifunctional ice storage air conditioning system in a confined mine refuge chamber, Energy 141 (2017) 964-974, https://doi.org/10.1016/j.energy.2017.09.123.

[38] X. Gao, Y. Yuan, X. Cao, H. Wu, X. Zhao, D. Yan, Coupled cooling method and application of latent heat thermal energy storage combined with pre-cooling of envelope: temperature control using phase-change chair, Sust. Cities Soc. 42 (2018) 38-51, https://doi.org/10.1016/j.scs.2018.06.032.

[39] X. Gao, Z. Zhang, Y. Yuan, X. Cao, C. Zeng, D. Yan, Coupled cooling method for multiple latent heat thermal storage devices combined with pre-cooling of envelope: model development and operation optimization, Energy 159 (2018) 508-524, https://doi.org/10.1016/j.energy.2018.06.151.

[40] Y. Junling, Y. Luwei, W. Juan, M. Yuezheng, Z. Zhentao, Study on open-cycle carbon dioxide refrigerator for movable mine refuge chamber, Appl. Therm. Eng. 52 (2) (2013) 304-312, https://doi.org/10.1016/j.applthermaleng.2012.12.014.

[41] L. Yan, D. Yantek, M. Reyes, B. Whisner, J. Bickson, J. Srednicki, N. Damiano, E. Bauer, Cryogenic air supply for cooling built-in-place refuge alternatives in hot mine, Mining, Metallurgy & Exploration 37 (3) (2020) 861-871, https://doi.org/10.1007/s42461-020-00194-w.

[42] Y. Yuan, X. Gao, H. Wu, Z. Zhang, X. Cao, L. Sun, N. Yu, Coupled cooling method and application of latent heat thermal energy storage combined with pre-cooling of envelope: method and model development, Energy 119 (2017) 817-833, https://doi.org/10.1016/j.energy.2016.11.058.

[43] Z. Zhang, W. Guo, X. Gao, H. Wu, R. Mao, Investigation on temperature control based on cooled mine compressed air for mine refuge chamber with high-temperature surrounding rock, Int. J. Therm. Sci. 187 (2023) 108201, https://doi.org/10.1016/j.ijthermalsci.2023.108201.

[44] M. Khabbaz, B. Benhamou, K. Limam, P. Hollmuller, H. Hamdi, A. Bennouna, Experimental and numerical study of an earth-to-air heat exchanger for air cooling in a residential building in hot semi-arid climate, Energy Build. 125 (2016) 109-121, https://doi.org/10.1016/j.enbuild.2016.04.071.

[45] X. Guo, H. Wei, X. He, J. Du, D. Yang, Experimental evaluation of an earth–to–air heat exchanger and air source

heat pump hybrid indoor air conditioning system, Energy Build. 256 (2022) 111752, https://doi.org/10.1016/j.enbuild.2021.111752.

[46] G.F. Frate, L. Ferrari, P. Sdringola, U. Desideri, A. Sciacovelli, Thermally integrated pumped thermal energy storage for multi-energy districts: integrated modelling, assessment and comparison with batteries, J. Energy Storage 61 (2023) 106734, https://doi.org/10.1016/j.est.2023.106734.

[47] M.T. Ameen, Z. Ma, A. Smallbone, R. Norman, A.P. Roskilly, Experimental study and analysis of a novel layered packed-bed for thermal energy storage applications: a proof of concept, Energy Conv. Manag. 277 (2023) 116648, https://doi.org/10.1016/j.enconman.2022.116648.

[48] K. Knobloch, Y. Muhammad, M.S. Costa, F.M. Moscoso, C. Bahl, O. Alm, K. Engelbrecht, A partially underground rock bed thermal energy storage with a novel air flow configuration, Appl. Energy 315 (2022) 118931, https://doi.org/10.1016/j.apenergy.2022.118931.

[49] K. Knobloch, T. Ulrich, C. Bahl, K. Engelbrecht, Degradation of a rock bed thermal energy storage system, Appl. Therm. Eng. 214 (2022) 118823, https://doi.org/10.1016/j.applthermaleng.2022.118823.

[50] N.B. Desai, M.E. Mondejar, F. Haglind, Techno-economic analysis of two-tank and packed-bed rock thermal energy storages for foil-based concentrating solar collector driven cogeneration plants, Renew. Energy 186 (2022) 814-830, https://doi.org/10.1016/j.renene.2022.01.043.

[51] X. Bai, Z. Tang, A numerical study of rock bed seasonal thermal storage used for mine ventilation, Sustain. Energy Technol. Assess. 50 (2022) 101867, https://doi.org/10.1016/j.seta.2021.101867.

[52] J.C.W.S. Shuai Zhu, Using seasonal temperature difference in underground surrounding rocks to cooling ventilation airflow: a conceptual model and simulation study, Energy Sci. Eng. 8 (10) (2020) 3457-3475, https://doi.org/doi.org/10.1002/ese3.619.

[53] X. Zhang, B. Bu, L. Liu, T. Cao, Y. Ke, Q. Du, Z. Han, Y. Duan, Study on temperature drop and cooling effect of cold wall for backfill body with embedded cold fluid tube, Int. J. Therm. Sci. 184 (2023) 107904, https://doi.org/10.1016/j.ijthermalsci.2022.107904.

[54] W. Guo, Z. Zhang, H. Wu, L. Ge, X. Liang, R. Mao, Experimental study on cooling and dehumidification performance of an ice storage air conditioner used in underground refuge chamber, Int. Commun. Heat Mass Transf. 146 (2023) 106930, https://doi.org/10.1016/j.icheatmasstransfer.2023.106930.

[55] Z. Zhang, W. Guo, H. Wu, L. Ge, Xing Liang, R. Mao, Thermal performance of an ice storage device for cooling compressed mine air in high-temperature mine refuge chambers, Appl. Therm. Eng. 233 (2023) 121101, https://doi.org/10.1016/j.applthermaleng.2023.121101.

[56] X. Gao, Y. Yuan, H. Wu, X. Cao, X. Zhao, Coupled cooling method and application of latent heat thermal energy storage combined with pre-cooling of envelope: optimization of pre-cooling with intermittent mode, Sust. Cities Soc. 38 (2018) 370-381, https://doi.org/10.1016/j.scs.2018.01.014.

[57] Q. Cao, M. Liu, X. Li, C. Lin, D. Wei, S. Ji, T.T. Zhang, Q. Chen, Influencing factors in the simulation of airflow and particle transportation in aircraft cabins by cfd, Build. Environ. 207 (2022) 108413, https://doi.org/10.1016/j.buildenv.2021.108413.

[58] J. Lin, Y. Kong, L. Zhong, Optimization of environment control system for narrow sleeping space in underground shelters, Energy Build. 263 (2022) 112043, https://doi.org/10.1016/j.enbuild.2022.112043.

[59] T. Wu, C. Lei, On numerical modelling of conjugate turbulent natural convection and radiation in a differentially heated cavity, Int. J. Heat Mass Transf. 91 (2015) 454-466, https://doi.org/10.1016/j.ijheatmasstransfer.2015.07.113.

[60] M. Boulet, B. Marcos, M. Dostie, C. Moresoli, Cfd modeling of heat transfer and flow field in a bakery pilot oven, J. Food Eng. 97 (3) (2010) 393-402, https://doi.org/10.1016/j.jfoodeng.2009.10.034.

[61] Z. Zhang, R. Day, K. Wang, H. Wu, Y. Yuan, Thermal performance analysis of an underground closed chamber with human body heat sources under natural convection, Appl. Therm. Eng. 145 (2018) 453-463, https://doi.org/10.1016/j.applthermaleng.2018.09.068.